

Identification and parameter determination of F-type Herbig stars from LAMOST DR8

YUN-JIN ZHANG ^{1,2} A-LI LUO ^{1,2} BIWEI JIANG ³ WEN HOU ¹ FANG ZUO ¹ BING DU ¹ SHUO LI ^{1,2} AND
YONG-HENG ZHAO^{1,2}

¹ CAS Key Laboratory of Optical Astronomy, National Astronomical Observatories, Beijing 100101, China

² University of Chinese Academy of Sciences, Beijing 100049, China

³ Department of Astronomy, Beijing Normal University, Beijing 100875, China

(Received April 26, 2022; Revised July 21, 2022; Accepted)

Submitted to ApJ

ABSTRACT

We identify 20 F-type Herbig stars and provide a list of 22 pre-main-sequence candidates from LAMOST DR8. The effective temperature, distance, extinction, stellar luminosity, mass, and radius are derived for each Herbig star based on optical spectra, photometry, Gaia EDR3 parallaxes, and pre-main-sequence evolutionary tracks. According to spectral energy distributions, 19 F-type Herbig stars belong to Class II YSOs, and one belongs to the flat-spectrum class. Four have Spitzer IRS spectra, of which three show extremely weak polycyclic aromatic hydrocarbons emissions, and three with both amorphous and crystalline silicate emissions share the similar parameters and are at the same evolutionary stage. We detect a solar-nearby outbursting EXor Herbig star J034344.48+314309.3, possible precursor of a Herbig Ae star. Intense emission lines of H I, He I, O I, Na I, and Ca II originated from the rapid accretion during the outbursts are detected in its optical spectra, and silicate emission features are detected in its infrared spectrum. We also make a statistic analysis on the disk properties of all known Herbig stars using the defined infrared spectral indices (α_{J-K_S} and α_{K_S-W3}). The proportion of Herbig stars with moderate infrared excesses decreases as effective temperature increases. The majority of the precursors (F-, G-, or K- type) have moderate infrared excesses. Hotter Herbig stars tend to have a larger proportion with large infrared excesses. The trends may be due to the fact that hotter stars have larger areas of re-emitting dust, although there is some scatter due to the particularities of each disk.

Keywords: stars: pre-main sequence - stars: variables: T Tauri, Herbig Ae/Be

1. INTRODUCTION

Young stellar object (YSO) denotes a young star in its early stage of evolution. Pre-main-sequence (PMS) stars and protostars are the two subtypes of YSOs. Protostars with collapsing envelopes are deeply embedded in the parent molecular clouds and optically invisible (Lada 1987). Compared with the younger counterparts, after dust envelopes infalling, PMS stars with accretion disks are optically visible. When approaching the main-sequence stage, the circumstellar dust disk will even-

tually be dispersed by planet formation and radiation pressure from the central star.

Herbig Ae/Be stars (HAeBes) and T Tauri stars (TTs) are the two main types of PMS stars. The concept of TTs was defined as PMS stars with late spectral types (later than late F, Joy (1945); Herbig (1962); Bastian et al. (1983)). As the counterpart of TTs, HAeBes were first defined by Herbig (1960) as emission-line stars with a spectral type of A or earlier which are located in obscured regions and illuminate fairly bright nebula in the immediate vicinity. Subsequently, Strom et al. (1972) extended the HAeBes definition with additional properties, including infrared (IR) excess, time variation, linear polarization, and association with star-forming regions. Since then, the HAeBes data set has been enlarged by numerous studies over decades

Corresponding author: A-Li Luo

* lal@nao.cas.cn

(Finkenzeller & Mundt 1984; The et al. 1994; Vieira et al. 2003; Hernández et al. 2005; Zhang et al. 2006; Manoj et al. 2006; Baines et al. 2006; Sartori et al. 2010; Carmona et al. 2010; Alecian et al. 2013; Fairlamb et al. 2015; Chen et al. 2016; Vioque et al. 2018; Keller et al. 2019; Moura et al. 2020; Vioque et al. 2020; Pereira et al. 2021; Zhang et al. 2022; Vioque et al. 2022).

In early research, HAeBes are usually limited to PMS stars with A or B spectral types. But in more recent works, HAeBes are generally defined as PMS stars with intermediate mass (1.5 or $2-10 M_{\odot}$), and a few F-type Herbig stars at the early evolutionary stage in the PMS track have also been included. Keller et al. (2019) identified 13 HAeBes with spectral types ranging from early G to B in the Small Magellanic Cloud. Vioque et al. (2022) identified 128 Herbig stars based on spectra and Gaia EDR3 data, the spectra of which also range from early G to B.

As the bridge of typical HAeBes and TTs, research about F-type PMS stars is rare. Calvet et al. (2004); Lavail et al. (2017) defined a specified intermediate-mass T Tauri (IMTT) class with $1-4 M_{\odot}$. Nuñez et al. (2021) characterized the X-Ray emission of intermediate-mass PMS stars in the Carina Nebula. Actually, IMTTs are usually the precursors of the HAeBes, often of F type. Depending on the PMS evolutionary tracks (Tognelli et al. 2011; Bressan et al. 2012; Marigo et al. 2017), most of the F-type PMS stars will be able to become HAeBes eventually. To distinguish from traditional Herbig Ae/Be stars, we called these F-type PMS stars with stellar masses larger than $1.5 M_{\odot}$ as F-type Herbig stars. F-type PMS with stellar masses less than $1.5 M_{\odot}$ as F-type T Tauri stars. Despite the similar spectral types, ages are quite different. F-type Herbig stars are the precursors of HAeBes. Valegård et al. (2021) pointed out the timescales on evolving toward the main sequence are comparable to those of typical disk dissipation, and a full picture of disk dispersal must include these precursors. They analysed 49 precursors of young HAeBes with spectral types ranging from F to K3 in literature, and found the polycyclic aromatic hydrocarbons (PAH) detection frequency of the precursors is different from that of HAeBes and TTs. They also suggested gaps and spirals are present around these younger precursors of HAeBes.

According to the SIMBAD (keyword TT* and Ae*), the number of known F-type PMS stars is 60, far less than that of HAeBes and TTs. From the 2.53 million F-type spectra of the Large Sky Area Multi-Object Fiber Spectroscopic Telescope (LAMOST) DR8, we have a chance to discover more F-type PMS stars. Fortunately, 20 F-type Herbig stars were identified, along with 22

PMS candidates. The effective temperature, distance, extinction, stellar luminosity, mass, and radius were derived for each Herbig stars based on optical spectra, photometry, Gaia EDR3 parallaxes, and pre-main-sequence evolutionary tracks. According to spectral energy distributions (SEDs), 19 F-type Herbig stars belong to Class II YSOs, and one belongs to the flat-spectrum class.

The outline of this paper is as follows. In Section 2, we introduce our data and our catalogs. In Section 3, we make the sample selection and confirmation. In Section 4, we determine stellar parameters for our F-type Herbig stars. In Section 5, we make a further analysis on the Herbig stars. In Section 6, we detect a solar-nearby outbursting EXor Herbig star and discuss the disk properties of all known Herbig stars. A brief summary is provided in Section 7.

2. OBSERVATIONS

LAMOST is a reflecting Schmidt telescope located at the Xinglong Station of the National Astronomical Observatory, China ($40^{\circ}\text{N}, 105^{\circ}\text{E}$), with a mean aperture of 4.3 m and a field of view of 5° . The LAMOST spectrograph has two resolving modes, the low-resolution mode of $R \sim 1800$ and the medium-resolution mode of $R \sim 7500$. Until 2021 June, DR8¹ published more than 11 million low-resolution spectra covering 3690–9100Å and about 17.6 million single exposure (4.7 million coadded) medium-resolution spectra covering 4950–5350Å and 6300–6800Å.

The data we used includes 2,538,636 low-resolution spectra of F-type stars classified by LAMOST 1D-pipeline (Luo et al. 2015) based on LAMOST DR8 v1.0. All spectra have been reduced through LAMOST 2D-pipeline with telluric absorption corrected, sky background subtracted, and flux and wavelength calibrated (Bai et al. 2017).

All the catalogs can be downloaded **via China-VO:** <https://nadc.china-vo.org/res/r101135/>.

3. SAMPLE SELECTION

3.1. Criterion

The determination of circumstellar dust disk is essential for the identification of PMS stars. The main features of circumstellar disk on optical and infrared bands are the wide H α emission (gaseous disk) and the apparent infrared excess (dust disk). Zhang et al. (2022) proposed an updated criterion to search for HAeBes and identified 71 HAeBes from LAMOST DR7. We used a similar method to search for F-type PMS stars. The

¹ <http://www.lamost.org/dr8/>

criterion on IR excess for HAeBes proposed by Zhang et al. (2022) is as follow.

1. HAeBes are located in the defined region on either color-color diagram.
 - (a) $(K_S-W1, H-K_S)$ diagram
 $(H - K_S)_0 > 0.4$ and $(K_S - W1)_0 > 0.8$
 - (b) $(H-K_S, J-H)$ diagram
 $(J - H)_0 < 1.625 \times (H - K_S)_0 - 0.1$
 $(J - H)_0 > 0.58 \times (H - K_S)_0 - 0.24$
 $(J - H)_0 > -0.9 \times (H - K_S)_0 + 0.75$
2. HAeBes are located in the defined region on the $(W2-W3, W1-W2)$ diagram.
 $(W2 - W3)_0 > 2.0$
 $(W1 - W2)_0 > 0.25$
 $(W1 - W2)_0 < 0.9 \times (W2 - W3)_0 - 0.25$
 $(W1 - W2)_0 > -1.5 \times (W2 - W3)_0 + 2.1$
3. The target is an explicit point source on the WISE images of all four bands.

3.2. Data acquisition and confirmation

Our initial catalog consists of 2,538,636 low-resolution spectra of F-type stars classified by the LAMOST 1D pipeline. The primary method of LAMOST 1D pipeline is the Chi-square matching with the templates of Wei et al. (2014). The pipeline is designed for batch processing of enormous spectra instead of a single target. Thus it is not surprising that some non-F type spectra may be wrongly classified as F-type stars by the 1D pipeline. The poorly recognized spectra may be earlier or later than the F type, or the source may be not even a star when the quality of the spectrum is quite terrible in some extreme cases. It should be noted that all spectra have not been checked before being applied to the IR criterion.

3.2.1. Data acquisition

We retrieved the IR photometry from the AllWISE source catalog (Wright et al. 2013). As part of the on-line point source catalog, a match to the 2MASS point source catalog (Cutri et al. 2003; Skrutskie et al. 2006) is automatically included, and we retrieved these data as well. To exclude the possible unreliable photometry, we adopted the criteria of photometry quality recommended by Cutri et al. (2003); Wright et al. (2013); Xue et al. (2016). In total, we got 1,965,114 entries with $J < 15.8$, $H < 15.1$, $K_S < 14.3$, $W1 < 17.1$, and $W2 < 15.7$ mag.

3.2.2. Candidates

Extinction mainly consists of two components, interstellar extinction, and circumstellar extinction. Extinction will make a star appear redder and extinction correction will reveal its bluer nature. To include as many PMS candidates as possible for the further investigation and avoid the unnecessary uncertainty of extinction correction, no extinction correction has been taken before the candidate searching.

We applied the first restriction based on the $(H-K_S, J-H)$ and $(K_S-W1, H-K_S)$ color-color diagrams to the whole entries. 712 PMS candidates were retrieved. As shown in Figure 1, 139 candidates located in the defined region on both two color-color diagrams are marked with blue dots, and 573 candidates located in the defined region on either diagram are marked with red dots. Black dots represent the sources ruled out according to the first restriction.

We applied the second restriction based on the $(W2-W3, W1-W2)$ color-color diagram. As extinction correction had not been applied, more PMS candidates should be included for the further inspection. We took the only one constraint $(W1 - W2)_0 > 0.25$ instead of the four constraints in the second restriction shown as the blue lines in Figure 2. Finally, 153 F-type PMS candidates were retrieved shown as the star marks in Figure 2. The wide distribution of $(W2 - W3)$ values in the excluded sources may be the consequence of falsely detected W3 values. When referred to the WISE images, these sources are usually too faint to be discerned on W3 band. Uncorrected interstellar extinction may also contribute to the scatter slightly, but it is not likely to be the main factor.

3.2.3. Candidate refining and confirmation

The sample of the 153 PMS candidates is undoubtedly contaminated by some fake sources, such as possible galaxies, quasi stellar objects, etc. Candidate refining consists of two procedures based on images and spectra, respectively.

The first step is the quality inspection of photometry based on the WISE images. As is recommended by Koenig & Leisawitz (2014), visual inspection is the most precise way to discern possible fake sources. To eliminate the fake sources in the WISE photometric data during YSO searching in large data set, Koenig & Leisawitz (2014) provided an empirical photometric filtration scheme (uncertainty/signal-to-noise/chi-squared criteria) and Marton et al. (2019) suggested a Random Forest method, both of which are based on the result of the visual inspection. Considering the accuracy and

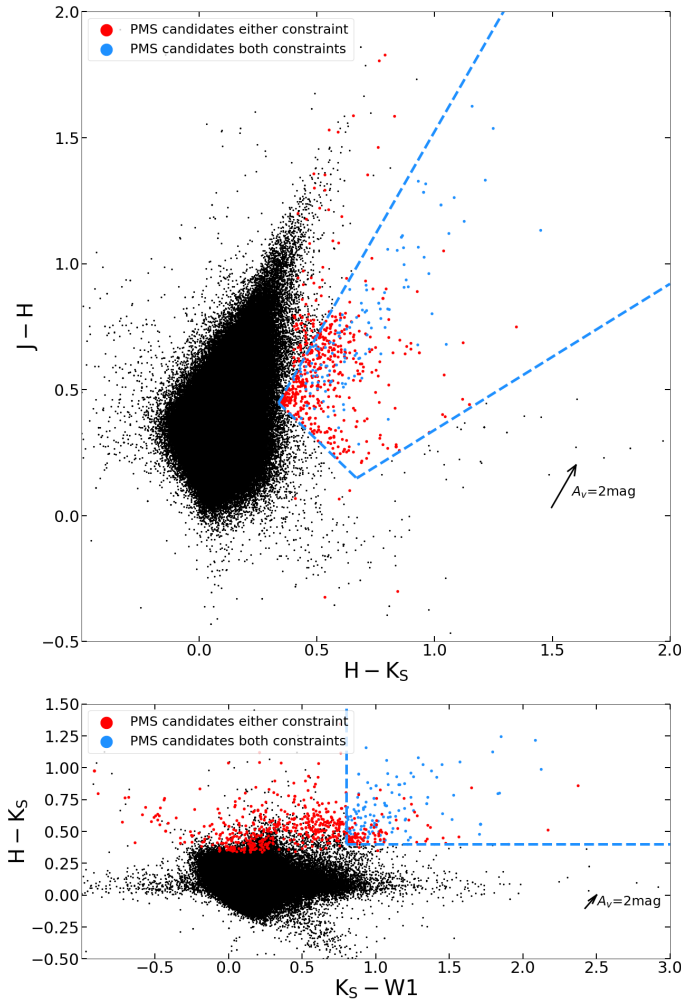


Figure 1. The result of the first restriction, namely ($H-K_S, J-H$) and ($K_S-W1, H-K_S$) diagram. Blue and red dots are the pre-main-sequence candidates. Blue ones are the common candidates through two diagrams, while red ones are only recognized as candidates in either diagram. The black dots represent the sources ruled out according to the first restriction.

our moderate data size, we visually inspected the WISE images of the 153 PMS candidates on all four bands.

The second step is visual inspection of optical spectra. We removed possible galaxies and picked out spectra with discernable photospheric continuum as the final candidates for the further confirmation.

We made the confirmation progress one by one based on the WISE images and optical spectra. When a source is a distinct point source on four bands of the WISE images and has good-quality spectra free of intense nebula emissions ($[\text{NII}]6549, 6583\text{\AA}$, $[\text{SII}]6717, 6731\text{\AA}$, $[\text{OIII}]4959, 5007\text{\AA}$), we confirm it as a PMS star (location on the HR diagram is shown in Figure 5). When a source is affected by the environment (molecular clouds

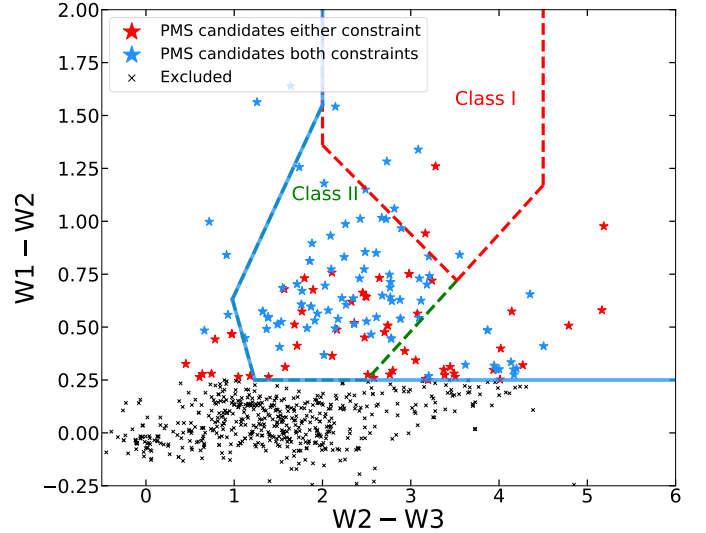


Figure 2. The result of the second restriction, namely ($W2-W3, W1-W2$) diagram. The star marks represent the pre-main-sequence candidates. The cross marks are the sources excluded according to the second restriction. All the star and cross marks are from the blue and red dots in Figure 1. The regions of Class I and II YSOs proposed by Koenig & Leisawitz (2014) are marked with red and green lines, respectively. The blue lines represent the constraints of H A e Bes defined by Zhang et al. (2022).

or bright nearby stars) on the WISE images, its spectra are contaminated by intense nebula emission lines or its spectra are greatly affected by noise, we confirm it as a PMS candidate. We got 21 PMS stars and 10 PMS candidates along with one evolved star J191512.12+394250.5, a well-known post-AGB binary (IRAS 19135+3937, Bollen et al. (2019); Oomen et al. (2019)).

We also checked the sources ruled out according to the first restriction but still meet the second restriction to avoid possible omissions. 12 additional PMS candidates were retrieved. All of the 12 candidates locate close to the selected region defined by the upper panel of Figure 1.

Finally, we got 21 PMS stars and 22 PMS candidates in total. As shown in Figure 3, we plotted the WISE pseudo-color images² ($W1$ in blue, $W2$ in green, and $W4$ in red) of the 21 PMS stars.

We also measured the FWHM of $H\alpha$ emission lines. The average FWHM of 21 PMS stars is 7.43\AA , corresponding to 339 km s^{-1} . The average FWHM of 22 PMS candidates is 6.49\AA , corresponding to 296 km s^{-1} . Besides, the 22 PMS candidates listed in Table

² <https://irsa.ipac.caltech.edu/applications/wise/>

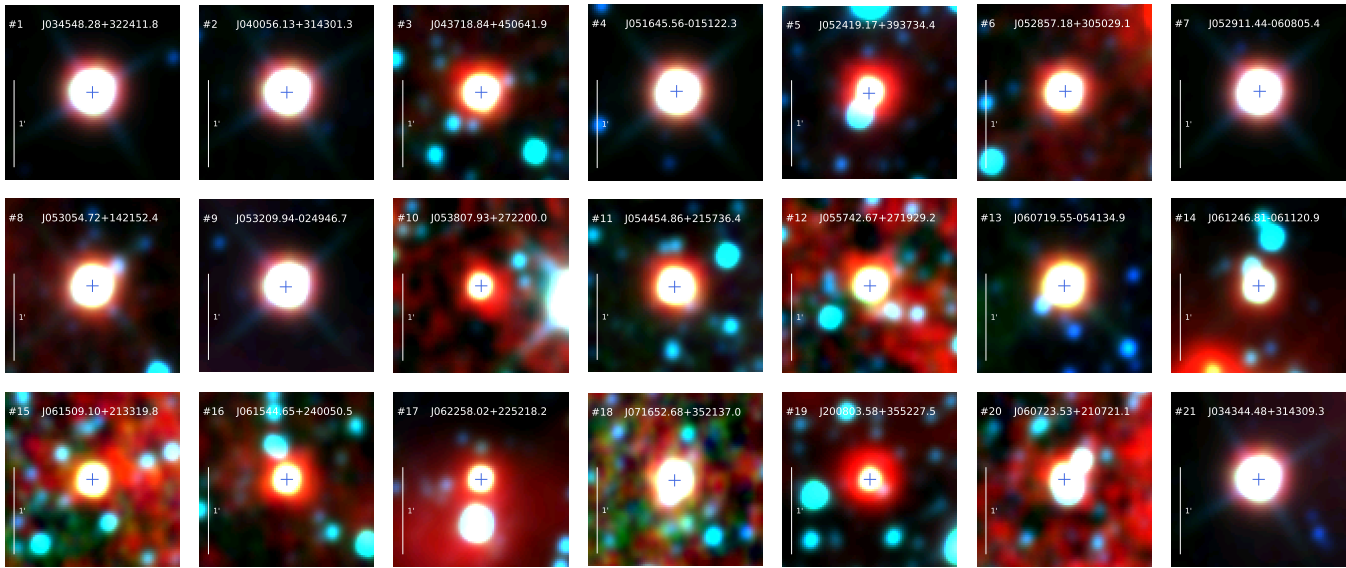


Figure 3. WISE pseudo-color images (W1 in blue, W2 in green, and W4 in red) of our 20 F-type Herbig stars and #21 (an outbursting EXor Herbig star, possible precursor of a Herbig Ae star). The target is marked with a blue cross in the middle of each image. All images are cut as $2' \times 2'$. The linear stretch range is from 5% to 95%.

A are not included in the following analysis. It should be noted that 21 PMS stars were retrieved, of which 20 are F-type Herbig stars as the main focus, and one is an outbursting EXor Herbig star discussed in Section 6.1.

4. STELLAR PARAMETERS

This section aims to determine the stellar parameters, such as the effective temperature, distance, reddening, stellar luminosity, mass, age, and radius. The parameters were determined by combining the LAMOST spectra, stellar model atmosphere grids, photometry, Gaia EDR3 parallaxes, and pre-main-sequence evolutionary tracks.

4.1. Effective temperature

A Chi-square match method was taken to determine the effective temperature (T_{eff}). The stellar model referenced is the synthetic Castelli & Kurucz model³ provided by Castelli & Kurucz (2003). The temperature grid we took is from 5600 K (typical temperature for G4) to 7500 K (typical temperature for A8) with the step of 100 K. The typical surface gravity $\log(g)$ of PMS stars is 3.5–4.5, and the value of $\log(g)$ between 3.5 and 4.5 does not have a significant effect on the spectra of the Castelli & Kurucz model (compared in the same T_{eff}). Thus, we adopted $\log(g)=4.0$ for the model spectra. We also assumed solar metallicity and adopted the abundance $[M/H]=0.0$.

To determine the optimum wavelength range for stellar parameter estimation, we compared two different wavelength ranges, one with the full range of 3800 – 9000Å, the other with H α and H β line masked which might be greatly influenced by emission lines (keeping 3800 – 4800Å, 4900 – 6500Å, and 6600 – 9000Å). Result turns out that the former is better by checking the fitting results with two ranges. We suggest that the wings of H α and H β profiles may provide valuable information during model fitting despite the emission cores may bring in some interferences. The line wings of Balmer lines were used in previous HAeBes works. For example, Wichittanakom et al. (2020) determined the effective temperature and surface gravity of HAeBes by comparing the wings of the observed hydrogen Balmer lines with model spectra. Finally, the wavelength coverage adopted for fitting is 3800 – 9000Å. It should be noted that rotational velocity was not taken into account because the low resolution and inaccurate rotational velocities may also bring in larger uncertainties.

We reduced the high-resolution model spectra ($R \sim 50,000$) into the same resolution as LAMOST ($R \sim 1800$). We also manually checked and corrected the ‘redshift’ z provided by LAMOST pipeline. We normalized the flux of both observed and synthetic spectra using the same method as follows.

$$F_i = \frac{f_i}{\sqrt{\frac{\sum f_i^2}{n}}} \quad (1)$$

³ <http://kurucz.harvard.edu/grids.html>

Table 1. F-type Herbig stars

No.	Designation	R.A. [degree]	Decl. [degree]	Specname	B [mag]	V [mag]
1	J034548.28+322411.8	56.45117	32.40329	spec-58423-TD034419N321717S01_sp04-055.fits	13.363	12.05
2	J040056.13+314301.3	60.2338894	31.7170317	spec-56981-HD040533N312949V01_sp03-164.fits	12.502	11.645
3	J043718.84+450641.9	69.3285	45.111639	spec-57299-GAC067N44B1_sp09-181.fits	15.016	14.133
4	J051645.56-015122.3	79.189855	-1.8562039	spec-56966-HD052428S022349V01_sp14-214.fits	11.354	10.747
5	J052419.17+393734.4	81.079912	39.626228	spec-57042-GAC084N40M1_sp10-118.fits		
6	J052857.18+305029.1	82.238266	30.841442	spec-55910-GAC_078N28_B1_sp12-049.fits spec-55907-GAC_079N29_B1_sp15-216.fits	16.037	14.702
7	J052911.44-060805.4	82.297671	-6.134844	spec-56617-VB081S05V2_sp08-011.fits	11.01	10.447
8	J053054.72+142152.4	82.7280228	14.3645656	spec-56958-HD052834N134044V01_sp09-154.fits	15.343	14.403
9	J053209.94-024946.7	83.0414269	-2.8296622	spec-56966-HD052428S022349V01_sp06-094.fits spec-57083-HD053813S011009V01_sp02-050.fits	12.345	11.495
10	J053807.93+272200.0	84.533079	27.366684	spec-56218-GAC083N27B1_sp04-114.fits	16.881	15.493
11	J054454.86+215736.4	86.228619	21.960137	spec-56680-GAC085N22B1_sp08-024.fits	15.309	14.394
12	J055742.67+271929.2	89.427826	27.324787	spec-56350-GAC089N28V2_sp01-150.fits	15.55	14.529
13	J060719.55-054134.9	91.831464	-5.693037	spec-56683-HD060658S061209B_sp04-219.fits	16.671	15.783
14	J061246.81-061120.9	93.195058	-6.189147	spec-56671-VB092S06V2_sp09-048.fits	14.945	13.803
15	J061509.10+213319.8	93.787935	21.555504	spec-57753-GAC093N19M1_sp12-133.fits spec-56983-GAC093N22M1_sp08-207.fits		
16	J061544.65+240050.5	93.936066	24.014044	spec-56609-GAC093N22M1_sp09-057.fits		
17	J062258.02+225218.2	95.741764	22.871742	spec-56658-GAC096N23B2_sp05-057.fits		
18	J071652.68+352137.0	109.21954	35.360292	spec-57104-GAC107N36B2_sp07-191.fits	15.014	14.535
19	J200803.58+355227.5	302.0149308	35.8743108	spec-57652-HD195955N370234B01_sp06-214.fits	15.367	14.426
20	J060723.53+210721.1	91.848052	21.122555	spec-56983-GAC093N22M1_sp02-136.fits		

NOTE—The ‘No.’ column is the sequential identifier of our F-type Herbig stars. The ‘Specname’ column is the FITS name of each spectrum. The B- and V- band photometry are from the APASS.

F_i is the normalized flux and f_i represents the flux before normalization. n is the total number of sampling points. The denominator represents the root-mean-square of flux.

We used an empirical five-degree polynomial for pseudo-continuum normalization, and we compared the spectral lines between our observed spectra and synthetic spectra during the model fitting progress to avoid flux calibration error caused by LAMOST data reduction.

For each spectrum, we made the fitting process at each sampling point of the grid (5600 K–7500 K, 100 K for step) and calculated the corresponding chi-square value. Besides the quantitative Chi-square values, we also visually checked the matching results based on published spectral standards (Digital Spectral Classification Atlas by Gray ⁴, Gray & Corbally (2009)). In most cases, the

optimal matching has the minimum Chi-square value. But when the quality of spectrum is not good enough such as seriously contaminated by noise, T_{eff} with minimum Chi-square value tends to be lower than the optimal matching. Noise strengthens the profile of metal lines and misleads the Chi-square value. In F-type spectra, metal lines enhance as temperature falls. Thus, visual inspection based on published spectral standard is also necessary.

The uncertainties of T_{eff} are set to be the step of grid, namely 100 K in most cases. For the spectra with low signal-noise ratio, the uncertainties are set to be double, namely 200 K. As shown in Figure 4, we used the pseudo-continuum of the best-fitting Castelli & Kurucz model to correct for the reddening along with the instrumental error, and plotted the optical spectra (blue) of 20 F-type Herbig stars, with the best-fitting Castelli & Kurucz model (gray) superposed. It should be noted that the LAMOST spectra are joint with the blue and red arms processed by different CCDs. Thus, in some

⁴ <http://ned.ipac.caltech.edu/level5/Gray/frames.html>

cases, such as #6 and #14, match on the joint place may not be good enough as others. Besides the joint place, the instrumental error is another cause. For example, the wave-like structure between 7200Å and 8000Å in the spectrum of #19 is due to the instrumental error rather than the intrinsic features. But these issues have little influence on our general Chi-square fitting method using the spectral lines.

4.2. Distance

To estimate extinction and stellar luminosity, and to make the further SED analysis, the distance information is essential. Gaia EDR3 provided full astrometric data for 1.468 billion sources, including positions, parallaxes and proper motions (Lindgren et al. 2021). We obtained the Gaia EDR3 parallax to each star. We estimated the distances by inversion of the parallaxes for 15 stars with $\sigma(\varpi)/\varpi \leq 0.1$. For five stars with $0.1 \leq \sigma(\varpi)/\varpi \leq 1.2$ (#5, #13, #15, #16, and #20), we adopted the geometric distances from Bailer-Jones et al. (2021).

4.3. Extinction and Luminosity

We collected B- and V- band photometry for 15 stars from the AAVSO Photometric All Sky Survey (APASS). With the TOPCAT tool provided by Taylor (2005) and the Vizier, 14 of them were collected from APASS DR9 (Henden et al. 2016) and a single one #18 was collected from UCAC4 (Zacharias et al. (2012), gathered from APASS DR6). Five stars without the APASS photometry (#5, #15, #16, #17, and #20) were managed with the SED fitting method described as the second part in this section.

4.3.1. 15 stars with the APASS photometry

We obtained the intrinsic Johnson-Cousins color $(B - V)_{intrinsic}$ and V-band bolometric correction BC_V for each spectral class from Table 6 of Pecaut & Mamajek (2013). $E(B - V)$ was derived from the observed color $(B - V)_{observed}$ and the intrinsic one $(B - V)_{intrinsic}$. We adopted total-to-selective extinction $R_V = 3.1$ for all stars (except #13 with large IR excess, where $R_V = 5$ was adopted as suggested by Hernández et al. (2004), Section 5.1 for details). We derived the absolute magnitude M_V with V-band photometry, A_V , and the distance d . Then we derived the absolute bolometric magnitude M_{bol} according to $M_{bol} = M_V + BC_V$. With the absolute bolometric magnitude of the Sun $M_{bol,\odot} = +4.74$, stellar luminosity L was derived in the unit of the solar luminosity L_\odot . The uncertainty of stellar luminosity was derived from the uncertainties of T_{eff} , V-band photometry, and distance.

$$M_V = V - A_V - 5 \log_{10} \left(\frac{d}{10pc} \right) \quad (2)$$

$$\log_{10} \frac{L}{L_\odot} = \frac{M_{bol,\odot} - M_{bol}}{2.5} \quad (3)$$

4.3.2. 5 stars analyzed with the SED fitting method

Five stars without the APASS photometry were analyzed with the SED fitting method assisted by the online tool Virtual Observatory SED Analyser (VOSA)⁵, developed by the Spanish Virtual Observatory. Guzmán-Díaz et al. (2021) made a study of 209 HAeBes gathered from literature, based on the results of VOSA. It should be noted that the best-fit output of VOSA is highly relevant to the input ranges of parameters, especially the T_{eff} , distance, and extinction. In most cases, the three parameters above always degenerate with each other. Benefiting from the known T_{eff} range from LAMOST spectra and the known distance range from Gaia EDR3 parallaxes, the VOSA output A_V and L are convincing.

We included photometric data from Gaia EDR3 (Riello et al. 2021), 2MASS (Skrutskie et al. 2006), and WISE (Wright et al. 2010). According to Guzmán-Díaz et al. (2021), photometry at wavelength shorter than U band or longer than J band should not be used to fit the photospheres for the possible excess due to the accretion and dust emission. Considering our T_{eff} uncertainties are 100 or 200 K and the grid step of the model is 250 K, Gaia EDR3 photometry alone (G_{BP}, G, G_{RP}) is adequate for fitting.

We adopted the same atmosphere model as mentioned in Section 4.1 for the SED fitting, namely Castelli & Kurucz model. The values of $\log(g)$ and metallicity have little effect on the SED shape (Wichittanakom et al. 2020; Guzmán-Díaz et al. 2021; Vioque et al. 2022). We assumed the input model parameters $\log(g) = 4.0$ and $[M/H] = 0.0$. We adopted a Chi-square fit method and used the Chi-square instead of the reduced Chi-square. The best-fit A_V along with the stellar luminosity and uncertainty can be obtained as the output of VOSA. Uncertainty of the stellar luminosity provided by VOSA is supposed to be mainly attributed to the input uncertainty of distance.

4.4. Stellar Mass, Age, and Radius

We used Hertzsprung-Russell (HR) diagram and pre-main-sequence evolutionary tracks to determine the stellar masses and ages for our PMS stars. Several famous evolutionary models were computed with different stellar evolutionary codes. The PARSEC (Bressan et al.

⁵ <http://svo2.cab.inta-csic.es/theory/vosa/>

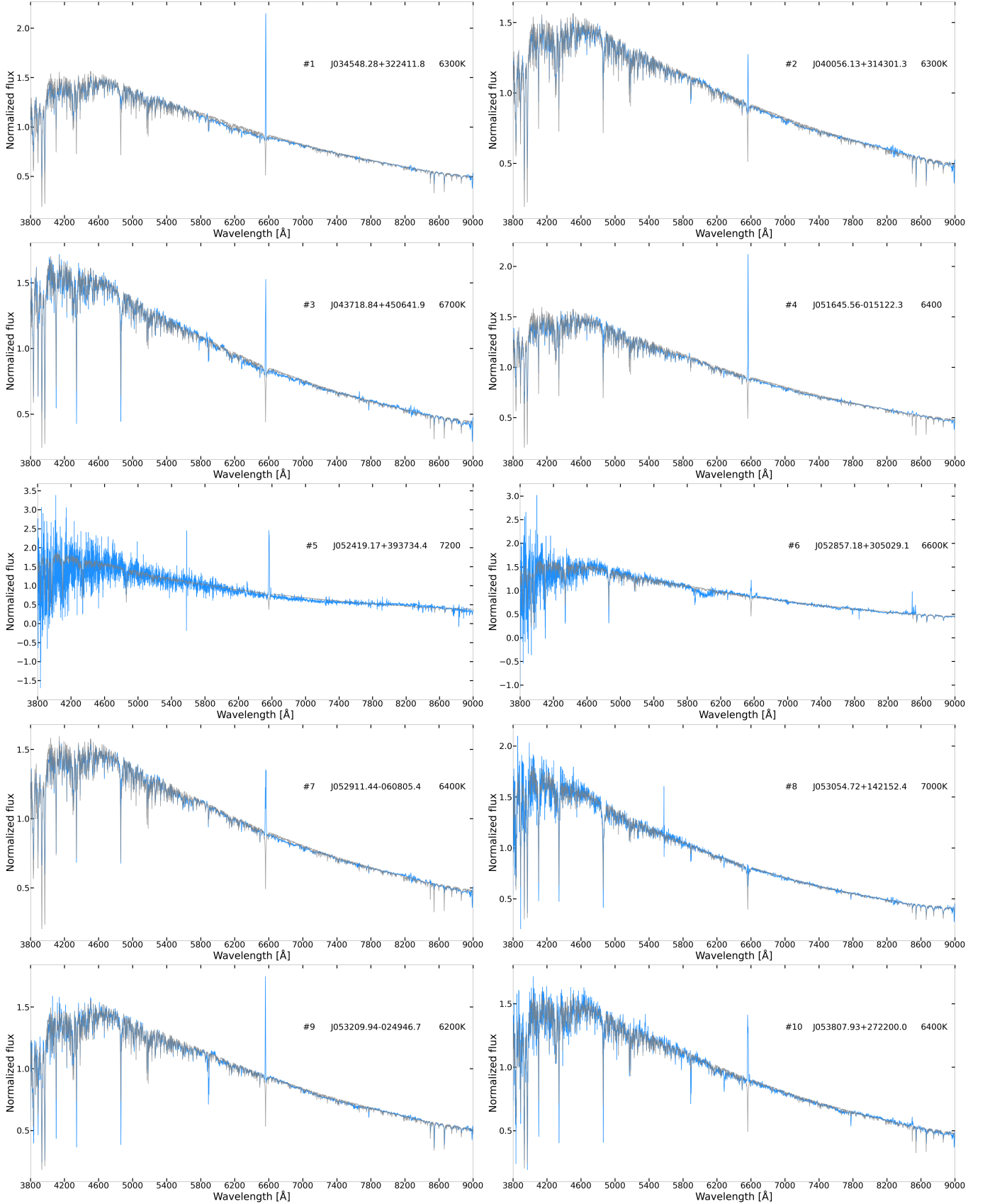


Figure 4. Optical spectra (blue) of our 20 F-type Herbig stars, with the best-fitting Castelli & Kurucz model (gray) superposed. The pseudo-continuum of the best-fitting Castelli & Kurucz model has been used in the optical spectrum to correct for the reddening along with the instrumental error.

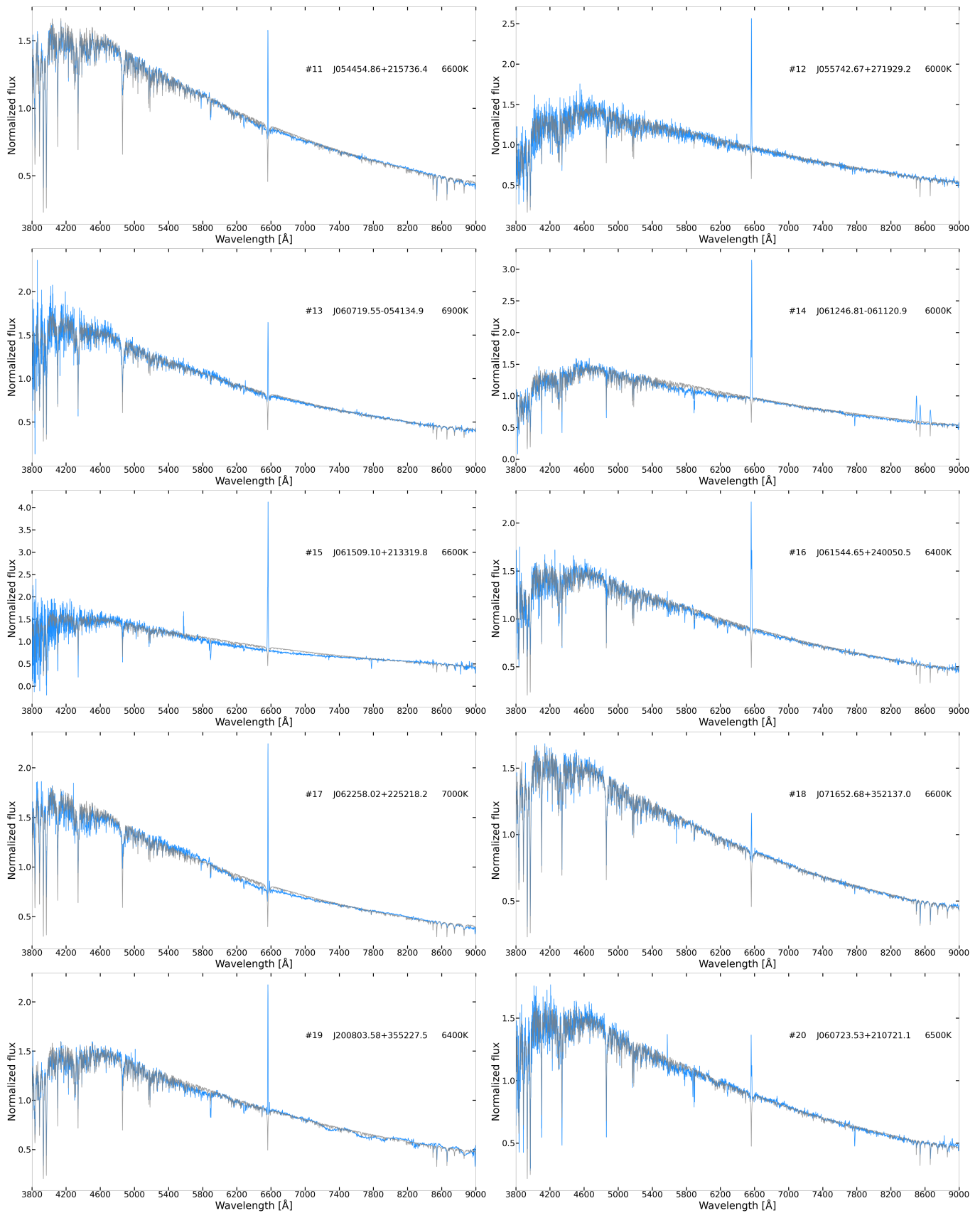


Figure 4. continued.

Table 2. Parameters of F-type Herbig stars

No.	Designation	T_{eff} [K]	SpType	Distance [pc]	A_V	$\log(L/L_{\odot})$	Mass [M_{\odot}]	Age [Myr]	Radius [R_{\odot}]
1	J034548.28+322411.8	6300^{+100}_{-100}	F6	$318.2^{+3.5}_{-3.5}$	$2.52^{+0.09}_{-0.09}$	$1.11^{+0.06}_{-0.07}$	$1.95^{+0.11}_{-0.10}$	$5.54^{+0.82}_{-0.72}$	$3.00^{+0.34}_{-0.31}$
2	J040056.13+314301.3	6300^{+100}_{-100}	F6	$370.0^{+3.7}_{-3.6}$	$1.11^{+0.09}_{-0.09}$	$0.83^{+0.06}_{-0.07}$	$1.58^{+0.08}_{-0.08}$	$9.43^{+1.47}_{-1.08}$	$2.19^{+0.24}_{-0.23}$
3	J043718.84+450641.9	6700^{+100}_{-100}	F2	$1156.2^{+26.3}_{-25.1}$	$1.56^{+0}_{-0.16}$	$1.00^{+0.05}_{-0.11}$	$1.68^{+0.06}_{-0.11}$	$8.60^{+1.44}_{-0.66}$	$2.34^{+0.21}_{-0.34}$
4	J051645.56-015122.3	6400^{+100}_{-100}	F5	$367.9^{+1.8}_{-2.8}$	$0.42^{+0}_{-0.09}$	$0.91^{+0.02}_{-0.05}$	$1.63^{+0.03}_{-0.05}$	$8.89^{+0.78}_{-0.65}$	$2.31^{+0.12}_{-0.19}$
5	J052419.17+393734.4	7200^{+200}_{-200}	F0	$6049.8^{+2348.1}_{-1674.4}$	3.50	$1.63^{+0.22}_{-0.48}$	$2.65^{+0.54}_{-0.85}$	$2.78^{+4.84}_{-1.08}$	$4.21^{+1.54}_{-1.90}$
6	J052857.18+305029.1	6600^{+100}_{-100}	F4	$1646.9^{+90.7}_{-81.7}$	$2.81^{+0.16}_{-0.12}$	$1.57^{+0.17}_{-0.15}$	$2.72^{+0.41}_{-0.33}$	$2.45^{+0.98}_{-0.77}$	$4.69^{+1.16}_{-0.84}$
7	J052911.44-060805.4	6400^{+100}_{-100}	F5	$355.8^{+4.1}_{-4.0}$	$0.29^{+0}_{-0.09}$	$0.94^{+0.03}_{-0.06}$	$1.68^{+0.04}_{-0.08}$	$8.28^{+1.07}_{-0.59}$	$2.41^{+0.16}_{-0.23}$
8	J053054.72+142152.4	7000^{+100}_{-100}	F1	$751.2^{+10.8}_{-10.5}$	1.86^{+0}_{-0}	$0.63^{+0.06}_{-0.06}$	$1.46^{+0.04}_{-0.04}$	$14.62^{+5.44}_{-0.01}$	$1.40^{+0.15}_{-0.13}$
9	J053209.94-024946.7	6200^{+100}_{-100}	F7	$350.5^{+2.5}_{-2.4}$	$0.99^{+0.09}_{-0.06}$	$0.80^{+0.10}_{-0.09}$	$1.58^{+0.13}_{-0.10}$	$9.19^{+1.65}_{-1.74}$	$2.19^{+0.36}_{-0.28}$
10	J053807.93+272200.0	6400^{+100}_{-100}	F5	$2285.7^{+212.4}_{-179.1}$	$2.84^{+0}_{-0.09}$	$1.56^{+0.08}_{-0.10}$	$2.77^{+0.19}_{-0.22}$	$2.27^{+0.54}_{-0.36}$	$4.91^{+0.63}_{-0.67}$
11	J054454.86+215736.4	6600^{+100}_{-100}	F4	$1360.7^{+42.2}_{-39.7}$	$1.50^{+0.16}_{-0.12}$	$1.01^{+0.13}_{-0.11}$	$1.71^{+0.18}_{-0.12}$	$8.23^{+1.57}_{-1.89}$	$2.45^{+0.48}_{-0.36}$
12	J055742.67+271929.2	6000^{+200}_{-200}	F9	$1720.3^{+103.5}_{-92.4}$	$1.43^{+0.09}_{-0.12}$	$1.15^{+0.11}_{-0.11}$	$2.22^{+0.18}_{-0.18}$	$3.62^{+0.93}_{-0.89}$	$3.48^{+0.73}_{-0.60}$
13	J060719.55-054134.9	6900^{+200}_{-200}	F1	$845.5^{+199.0}_{-131.6}$	$2.74^{+0}_{-0.20}$	$0.53^{+0.21}_{-0.16}$	$1.42^{+0.09}_{-0.09}$	$16.89^{+6.24}_{-3.89}$	$1.29^{+0.44}_{-0.28}$
14	J061246.81-061120.9	6000^{+200}_{-200}	F9	$749.3^{+48.5}_{-42.9}$	$1.80^{+0.09}_{-0.12}$	$0.87^{+0.12}_{-0.12}$	$1.77^{+0.18}_{-0.16}$	$6.40^{+1.78}_{-1.68}$	$2.52^{+0.58}_{-0.47}$
15	J061509.10+213319.8	6600^{+200}_{-200}	F4	$1803.1^{+197.5}_{-162.4}$	3.00	$0.72^{+0.08}_{-0.10}$	$1.45^{+0.04}_{-0.06}$	$13.54^{+1.80}_{-2.06}$	$1.75^{+0.29}_{-0.28}$
16	J061544.65+240050.5	6400^{+100}_{-100}	F5	$1920.3^{+1151.7}_{-681.9}$	3.00	$0.87^{+0.23}_{-0.54}$	$1.59^{+0.30}_{-0.37}$	$9.47^{+11.87}_{-3.36}$	$2.21^{+0.78}_{-1.06}$
17	J062258.02+225218.2	7000^{+100}_{-100}	F1	$1649.6^{+65.1}_{-60.3}$	3.00	$1.53^{+0.03}_{-0.03}$	$2.48^{+0.07}_{-0.09}$	$3.24^{+0.34}_{-0.22}$	$3.95^{+0.27}_{-0.26}$
18	J071652.68+352137.0	6600^{+100}_{-100}	F4	$2479.5^{+141.0}_{-126.6}$	$0.15^{+0.16}_{-0.12}$	$1.11^{+0.11}_{-0.09}$	$1.84^{+0.16}_{-0.12}$	$6.77^{+1.37}_{-1.25}$	$2.73^{+0.46}_{-0.34}$
19	J200803.58+355227.5	6400^{+100}_{-100}	F5	$2207.0^{+95.0}_{-87.5}$	$1.46^{+0}_{-0.09}$	$1.41^{+0.06}_{-0.09}$	$2.43^{+0.12}_{-0.16}$	$3.18^{+0.63}_{-0.37}$	$4.10^{+0.42}_{-0.50}$
20	J060723.53+210721.1	6500^{+100}_{-100}	F5	$2331.7^{+523.9}_{-454.6}$	2.00	$0.69^{+0.15}_{-0.24}$	$1.40^{+0.15}_{-0.09}$	$13.70^{+4.31}_{-3.32}$	$1.75^{+0.40}_{-0.46}$

NOTE—The ‘No.’ column is the sequential identifier of our F-type Herbig stars. The ‘ T_{eff} ’ column represents the stellar effective temperature derived from the best-fitting with Castelli & Kurucz model (Castelli & Kurucz 2003). The ‘SpType’ column is the spectral type of LAMOST low-resolution spectra derived from the corresponding T_{eff} . The ‘Distance’ column is the distance to the Sun, derived from the parallax from Gaia EDR3. The extinction A_V , stellar luminosity, mass, age, and radius columns are the determined results in this work.

2012; Marigo et al. 2017) tracks and isochrones were computed with the PAdova and TRieste stellar evolution code. The Pisa (Tognelli et al. 2011) PMS tracks and isochrones used the FRANEC evolutionary code. Despite slight differences, the well-tested stellar evolutionary models share the similar result. We adopted the latter one (the Pisa model, dedicated to PMS evolution) to estimate stellar masses and ages for our PMS stars. We adopted the solar chemical composition proposed by Tognelli et al. (2011), namely the metallicity $Z = 0.01377$, the initial helium abundance $Y = 0.2533$, the mixing length parameter $\alpha = 1.68$, and the initial deuterium abundance $X_D = 2.0 \times 10^{-5}$.

Using the interpolation with two closet points on the evolutionary tracks, stellar masses and ages were obtained. Uncertainties of masses and ages were derived from the uncertainties of T_{eff} and stellar luminosities. As shown in Figure 5, the blue dots are the 15 stars with the APASS photometry, and the orange dots are the five stars analyzed with the SED fitting method based on Castelli & Kurucz model and Gaia EDR3 photometry.

The Pisa tracks ($1.0 - 3.0 M_{\odot}$) and isochrones (1,3,5,7,10 Myr) are also presented. The evolutionary tracks shown in Figure 5 are limited up to $10^{1.5}$ Myr.

It should be noted that pre-main-sequence evolutionary tracks partially overlap with post-main-sequence tracks. However, lacking dusty stellar winds, infrared excess is not expected for single intermediate-mass stars that have evolved to sub-giants (Valegård et al. 2021).

16 stars with masses ranging from 1.58 to $2.77 M_{\odot}$ were confirmed as F-type Herbig stars, 6 of which (#5, #6, #10, #12, #17, and #19) have masses larger than $2 M_{\odot}$. Besides, #8, #13, #15, and #20 with masses about $1.5 M_{\odot}$ were also classified as F-type Herbig stars in consideration of the uncertainties. In summary, we got 20 F-type Herbig stars in this work.

Using the Stefan-Boltzmann law, stellar luminosity can be expressed as $L = \sigma T^4 \times 4\pi R^2$. Thus, the stellar radius R can be determined with the derived T_{eff} and stellar luminosity. The stellar luminosity and radius are both in the unit of the solar values.

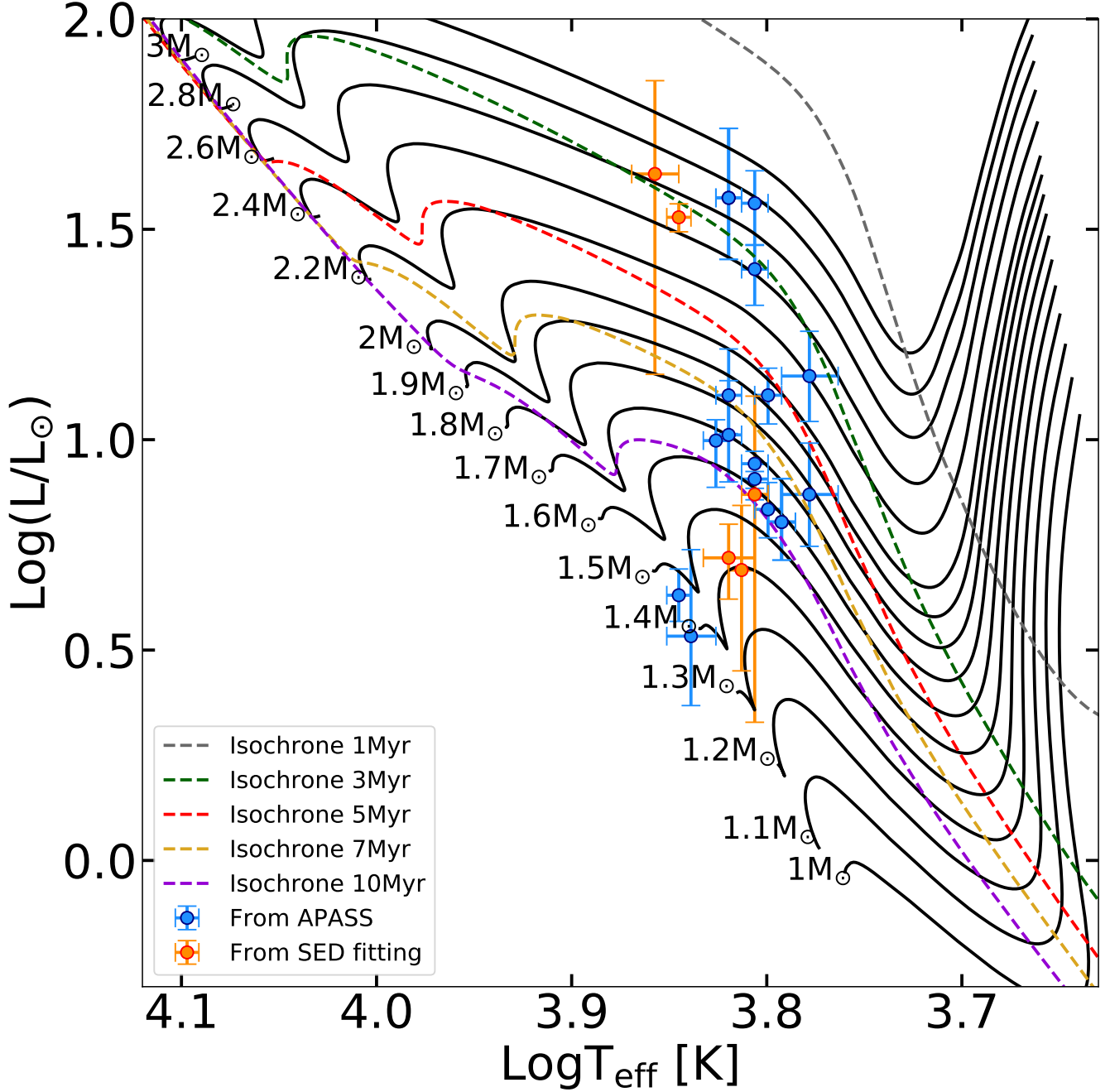


Figure 5. HR diagram of the 20 F-type Herbig stars. 15 stars with the APASS photometry are marked with the blue dots. Five stars analyzed with the SED fitting method based on Castelli & Kurucz model and Gaia EDR3 photometry are marked with the orange dots. The Pisa PMS evolutionary tracks and isochrones (Tognelli et al. 2011) are also presented. The evolutionary tracks shown are limited up to $10^{1.5}$ Myr. Model parameters are settled as Metallicity $Z=0.01377$, Helium abundance $Y=0.2533$, Mixing length $\alpha=1.68$, and initial deuterium abundance $X_D = 2.0 \times 10^{-5}$.

5. ANALYSIS

Detailed analysis of our F-type Herbig stars presented in this section are about SEDs, infrared spectra from Spitzer IRS enhanced product, and the records in literature.

5.1. Spectral Energy Distributions

The SEDs with Castelli & Kurucz model are shown in Figure 6. The photometric data included are from APASS DR9 (gray diamonds, corrected for reddening), Gaia EDR3 (blue dots, corrected for reddening), 2MASS

(violet squares, corrected for reddening), WISE (red dots, corrected for reddening), IRAS (orange triangles, IRA (1988a,b)), and AKARI (green diamonds, Ishihara et al. (2010)). The extinction law A_λ/A_V adopted for reddening correction is from Table 3 of Wang & Chen (2019). The Castelli & Kurucz model spectrum with corresponding T_{eff} is in black. In the SEDs of #6 and #10, the flux density of model spectra is little higher than Gaia EDR3 photometry. Possible variations are suggested to be the main cause. The extinctions and stellar luminosities of #6 and #10 were determined based on the APASS photometry rather than Gaia EDR3. Besides, as Guzmán-Díaz et al. (2021); Montesinos et al. (2009) pointed out, during the parameter determination of HAeBes, the photometry corresponding to the maximum of the stellar brightness (the star is likely to be less obscured) should be used in building the SEDs of variable stars.

The slope of SED can be used to discern the stage of YSO evolution. Lada (1987) first proposed the tripartite class system using the defined spectral index $\alpha = (d \log \lambda F_\lambda) / (d \log \lambda)$. λ means the wavelength and F_λ is the flux density at λ . The boundaries classified by Lada are Class I with $0 < \alpha \leq 3$, Class II with $-2 \leq \alpha \leq 0$, and Class III with $-3 < \alpha \leq -2$, and the slopes are determined between roughly 2 and 20 μm . Three categories represent three different evolutionary stages proposed by Lada (1987); Evans et al. (2009) (the envelope collapse as Class I, the accretion disk and star as Class II, and the disk dissipation during Class III). Andre et al. (1993) added a Class 0 with high ratio of submillimeter to bolometric luminosity. Greene et al. (1994) added a flat-spectrum class and formalized the modified system with the spectral index calculated between 2.2 and 10 μm . The modified 4-class system proposed by Greene et al. are detailed as follows. Class I has $\alpha \geq 0.3$, flat-spectrum class has $-0.3 \leq \alpha < 0.3$, Class II has $-1.6 \leq \alpha < -0.3$, and Class III has $\alpha < -1.6$. Calvet et al. (1994) explained the flat spectrum as infall inducing, in which material fall onto a disk rather than the central star. They suggested that many flat-spectrum sources should be YSOs surrounded by dust infalling envelopes of substantial mass.

We adopted the similar band taken, K_S (2MASS, 2.159 μm) and W3 (WISE, 11.5608 μm), and determined the slopes of our Herbig stars.

$$\alpha = \frac{\log(\frac{\lambda_{W3} F_{W3}}{\lambda_{K_S} F_{K_S}})}{\log(\frac{\lambda_{W3}}{\lambda_{K_S}})} \quad (4)$$

λ is the wavelength and F_λ is the flux density at λ . According to the modified 4-class system proposed by Greene et al. (1994), 19 F-type Herbig stars belong to

Class II YSOs, and the one #13 ($\alpha = 0.092$) belongs to the flat-spectrum class. #5 ($\alpha = -0.320$) is a Class II YSO but it is near the boundary of the flat-spectrum class. The relatively large extinction and the young age of #5 also agree with its early stage of disk evolution. However, #13 is not the case. #13 is bright on the IR bands and its derived age disagrees with its early stage of disk evolution indicated by the large IR excess. Despite taking a large value of total-to-selective extinction $R_V = 5$ as suggested by Hernández et al. (2004) for #13 rather than the standard $R_V = 3.1$, we might still underestimate its extinction and luminosity if the real R_V was even larger. It should be noted that the quality flags of #5 and #13 from the AllWISE are all excellent, ‘AAAA’ for ph_qual (photometric quality of each band) and no saturation has been detected. Similar to #5 and #13, some other Herbig stars with large IR excesses are also presented by Valegård et al. (2021); Guzmán-Díaz et al. (2021); Meeus et al. (2001). Statistic analysis of IR excesses can be seen as Section 6.2. In general, the mean slope of the 20 F-type Herbig stars in our work is -0.865, and the result of SED analysis is quite consistent with their PMS nature.

5.2. Infrared Spectra

The silicate dust grains are the main components of the circumstellar disks and usually have the size of sub-micron in diameter. Silicate has two subtypes depending on the lattice structure, namely amorphous silicate and crystalline silicate. High temperatures are required to thermally anneal and crystallize amorphous grains. Crystalline silicate grains are considered as tracers of the history of protoplanetary, circumstellar disk (Olofsson et al. 2009). Along with silicate, PAH molecules are also the tracers to probe the physical and chemical properties of protoplanetary disks (PAH molecules trace the gas disks). The infrared emission from PAH molecules is usually caused by stellar UV photons that excite electronic states in the PAH molecule, which subsequently de-excites through vibrational emission in stretching and bending mode resonances (Valegård et al. 2021).

We obtained infrared spectra⁶ for five stars (#1, #4, #7, #9, and #21) from the Infrared Spectrograph (IRS, Houck et al. (2004)) on the Spitzer Space Telescope (Werner et al. 2004). The IRS spectra are shown in Figure 7 with PAH and silicate emission features marked with light-color stripes. We set the threshold for a detectable feature when the peak is 1.02 over the continuum strength. It should be noted that the detected

⁶ <https://sha.ipac.caltech.edu/applications/Spitzer/SHA/>

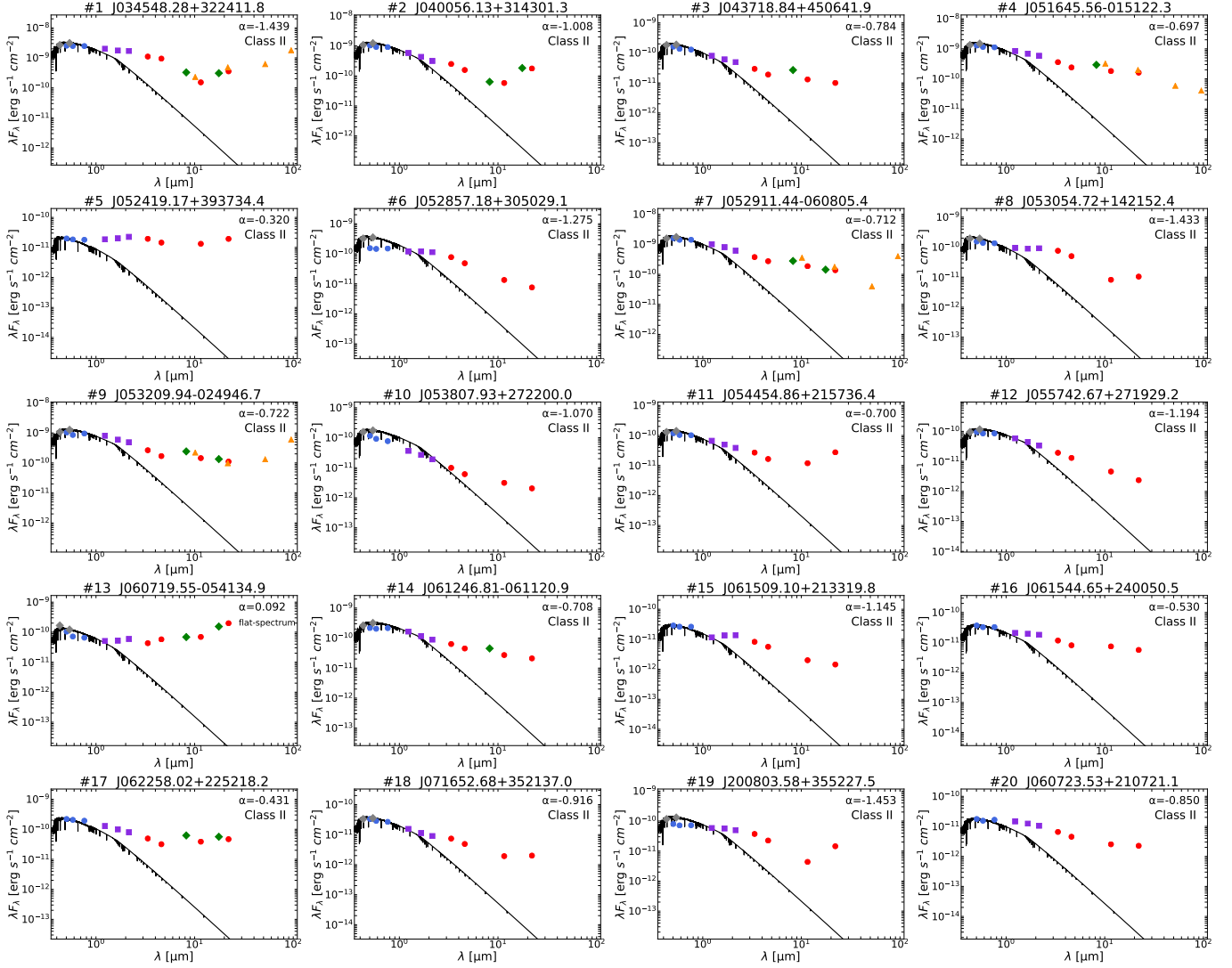


Figure 6. Spectral energy distributions of the 20 F-type Herbig stars. The photometric data included are from APASS DR9 (gray diamonds, corrected for reddening), Gaia EDR3 (blue dots, corrected for reddening), 2MASS (violet squares, corrected for reddening), WISE (red dots, corrected for reddening), IRAS (orange triangles), and AKARI (green diamonds). The Castelli & Kurucz model spectrum with the same T_{eff} is in black. The slope α provided is the spectral index α_{K_S-W3} .

crystalline silicate longer than $20 \mu\text{m}$ may be disturbed by noise.

The infrared spectra of #4, #7, and #9 are rather similar to each other, sharing the common features of amorphous silicate (peaking at 9.7 and $18.5 \mu\text{m}$) and crystalline silicate ($11.3 \mu\text{m}$). Coincidentally, they also have similar parameters (T_{eff} $6200\text{--}6400$ K, M_{star} $1.58\text{--}1.68 M_{\odot}$, Age $8.28\text{--}9.19$ Myr, Radius $2.19\text{--}2.41 R_{\odot}$). Considering they are at the same evolutionary stage, similar infrared spectra are also reasonable.

Dislike three ones above, #1 shows a rising infrared spectrum while #21 shows a flat one on the mid-infrared band. Besides the rising continuum peaking farther than mid-infrared, the only detectable features of #1 are the

extremely weak PAH emissions at 6.2 , 7.8 , and $11.3 \mu\text{m}$. The infrared spectrum of #21 shows the evidence of silicate, both amorphous and crystalline. The detected crystalline silicate features at 9.2 , 11.3 , 12.5 , 16.2 , 23.8 , 25 , 28.2 , and $33.6 \mu\text{m}$ are marked with light blue stripes.

5.3. Literature Records

Using the SIMBAD, we searched records in literature for our F-type Herbig stars, and only several of them have the records. According to literature, five stars (#1 EM* LkH α 330, #4 HD 290172, #7 V* V1650 Ori, #8 2MASS J05305472+1421524, and #9 V* RY Ori) have been recognized as HAEbes or TTs, and two stars

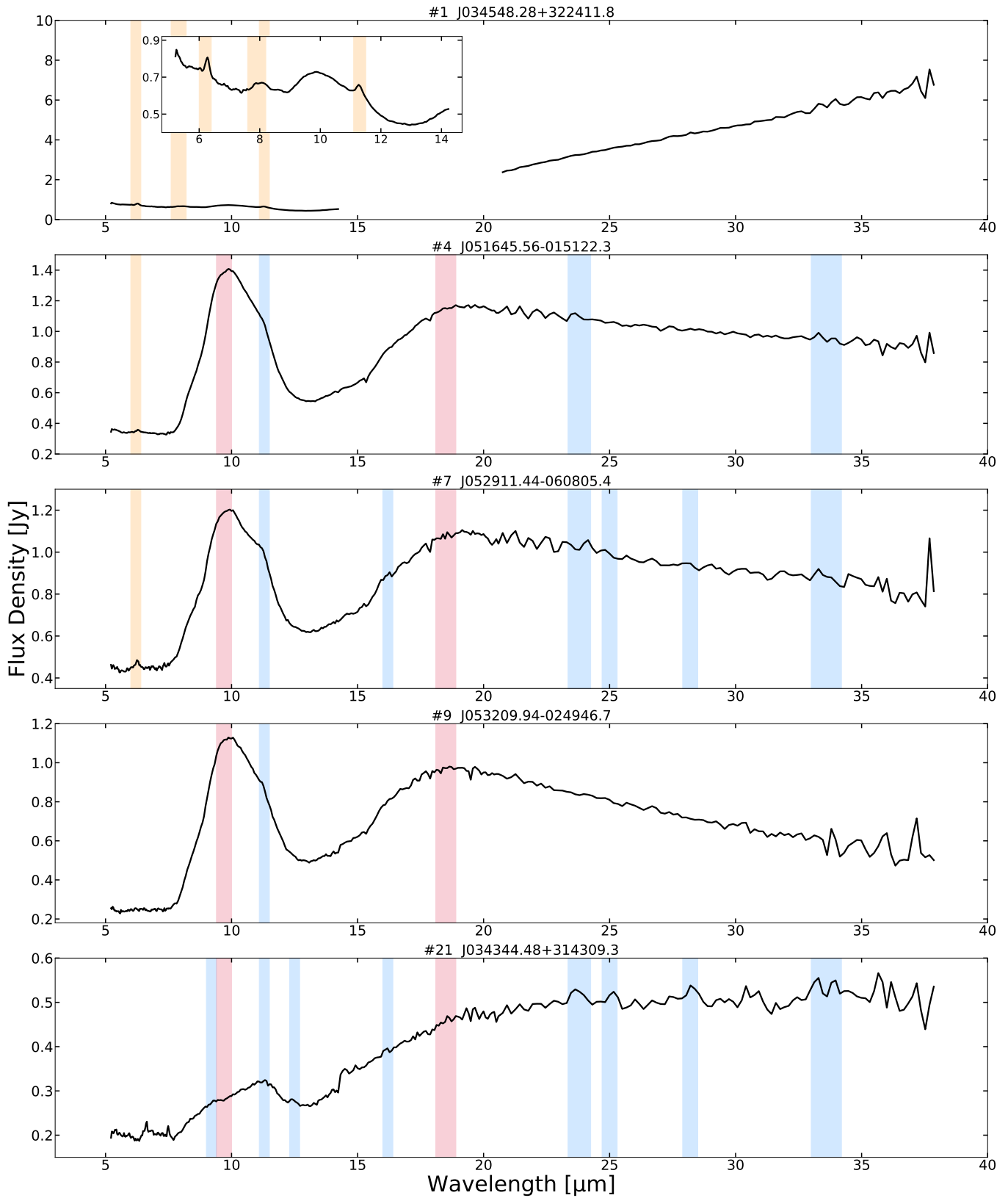


Figure 7. Five Herbig stars with Spitzer IRS spectra. The PAH emission features at 6.2, 7.8, and 11.3 μm are marked with light orange stripes. The amorphous silicate features peaking at 9.7 and 18.5 μm are marked with light crimson stripes. The detected crystalline silicate features are marked with light blue stripes.

(#2 IRAS 03577+3134 and #14 2MASS J06124681-0611208) have been classified as YSOs.

#1 is one of the most famous intermediate-mass T Tauri stars (Valegård et al. 2021; Varga et al. 2018; Seok & Li 2017; Hein Bertelsen et al. 2016; Banzatti & Pontoppidan 2015). It was first classified as a T Tauri star with the spectral type of F6 by Herbig (1977). Recently, Akiyama et al. (2016); Uyama et al. (2018) detected a spiral-like structure of the #1 disk suggesting a planet formation based on H-band linear polarimetric observations and H-, K_S-bands observations separately. Valegård et al. (2021) determined its parameters as 6240 K, 1.93 M_{\odot} , 4.66 Myr. In our work, we confirmed #1 as an F-type Herbig star (6300 K, 1.95 M_{\odot} , 5.54 Myr).

#4 is a known T Taur star which was first identified with a spectral type of G0 by Torres et al. (1995). In our work, we confirmed #4 as an F-type Herbig star (6400 K, 1.63 M_{\odot} , 8.89 Myr).

#7 is a famous HAeBe star, and it was first identified as a PMS star by Weintraub (1990). It was classified as a HAeBe star or an IMTT star by various works (Valegård et al. 2021; Villebrun et al. 2019; Acke & van den Ancker 2006; The et al. 1994; Gregorio-Hetem et al. 1992). Valegård et al. (2021) determined its parameters as 6160 K, 1.71 M_{\odot} , 6.20 Myr. In our work, we confirmed #7 as an F-type Herbig star (6400 K, 1.68 M_{\odot} , 8.28 Myr).

#8 was classified as a HAeBe star with a spectral type of F2 by Lee & Chen (2007). In our work, we confirmed #8 as an F-type Herbig star with the spectral type of F1 and the effective temperature of 7000 K. Considering its stellar mass (1.46 M_{\odot}) and uncertainty ($\pm 0.04 M_{\odot}$), #8 is on the boundary of Herbig stars.

#9 is another famous HAeBe star and numerous studies have included it (6120 K, 1.69 M_{\odot} , 6.65 Myr in Valegård et al. (2021), 6250 K, 1.58 M_{\odot} , 9.42 Myr in Guzmán-Díaz et al. (2021), and 6250 K, 1.542 M_{\odot} , 7.154 Myr in Vioque et al. (2018)). In our work, we confirmed #9 as an F-type Herbig star (6200 K, 1.58 M_{\odot} , 9.19 Myr).

#2 is a famous YSO, and it was first identified as a PMS star in an IRAS survey of the Taurus-Auriga molecular cloud by Kenyon et al. (1990). It was also studied by Beichman et al. (1992) with IRAS data. Casali & Eiroa (1996) further provided infrared CO absorption index for it. Recently, Azimlu et al. (2015); Rebull et al. (2011) made the studies to search for YSOs based on the WISE data, and #2 was also included in their work. In our work, we further identified #2 as an F-type Herbig star with 1.58 M_{\odot} .

#14 is a Class II YSO which was described as a PMS star with an optically thick disk (Gutermuth et al. 2009).

In our work, we further identified #14 as an F-type Herbig star with 1.77 M_{\odot} .

Heinze et al. (2018) provided the first catalog of variable stars measured by Asteroid Terrestrial-impact Last Alert System (ATLAS), including 427,000 probable variables. According to their work, five stars (#8 ATO J082.7280+14.3645, #13 ATO J091.8314-05.6930, #14 ATO J093.1950-06.1891, #15 ATO J093.7879+21.5555, and #16 ATO J093.9360+24.0140) were roughly classified as long-period variables (LPV) whose variation is in some sense irregular. It is worth mentioning that the only record in literature for #13, #15, and #16 is the variability nature.

5.4. Comparison with the LAMOST AFGK Catalog

We cross-matched our F-type Herbig stars with the online LAMOST LRS Stellar Parameter Catalog of A, F, G, and K stars (AFGK catalog), in which 16 of the F-type Herbig stars have stellar parameters T_{eff} , $\log(g)$, and $[M/H]$. In general, the provided effective temperatures agree with our values. Among the 16 F-type Herbig stars in the AFGK catalog, the mean value of $\log(g)$ (ranges from 3.744 to 4.374) is 4.01 dex, and the mean value of $[M/H]$ is -0.05 dex. The provided values of $\log(g)$ and $[M/H]$ are quite consistent with our assumptions, namely $\log(g)=4.0$ and the solar metallicity.

6. DISCUSSION AND SUMMARY

6.1. An outbursting EXor Herbig star

Besides the 20 F-type Herbig stars, we also detected an outbursting EXor Herbig star #21 J034344.48+314309.3 (R.A. 55.935352, Decl. 31.719259, IRAS F03406+3133, 2MASS J03434449+3143092), possible precursor of a Herbig Ae star.

#21 was first detected by Kraemer et al. (2003) in the observations of star-forming regions with the Midcourse Space Experiment. Then it was identified as a YSO candidate in the Perseus Molecular Cloud by Hsieh & Lai (2013); Evans et al. (2009) using the data from the c2d Spitzer Legacy project. Antonucci et al. (2014) suggested #21 is a bona fide young eruptive star (EXor) in the comparison study between the Spitzer and WISE data. They classified #21 as a flat-spectrum class protostar, and provided the stellar parameters (T_{eff} as 5718–5209 K, stellar mass as 2.1–1.5 M_{\odot} , stellar luminosity as 13–5.4 L_{\odot} , the first value refers to the best fit and the second to the model with a 20% higher chi-square). However, the stellar parameters of #21 are still in controversy. Cottaar et al. (2014) provided a peculiar value (868 K) as the T_{eff} for #21 with the forward modeling approach based on the spectra of the Apache Point Galactic Evolution Experiment (APOGEE). Also using

the high-resolution H-band spectra of APOGEE, [Chojnowski et al. \(2015\)](#) identified it as a Be star (ABE-149) with HI Brackett series emission along with emissions of FeII 16878, CI 16895, MgI 15753 and 15770. However, [Azimlu et al. \(2015\)](#) used a Bayesian Monte Carlo SED fitting method and estimated the stellar mass and age for #21 as $0.8 M_{\odot}$ and 1.05 Myr. Subsequently, [Chojnowski et al. \(2017\)](#) excluded #21 from their classical Be study and agreed with the young nature proposed by [Azimlu et al. \(2015\)](#). No available optical spectra for #21 before the LAMOST.

Seven low-resolution spectra for #21 are available from LAMOST DR8 observed between January 28 and December 6 in 2013. The single-exposure and coadded spectra are shown as Figure 8. Besides the intense emission lines of H α , HI Paschen series, and CaII triplet, we also detected obvious HeI 5877, 6680, OI 6302.046, 6365.536, and NaI 5891.583, 5897.558. Typical evidences, especially the intense HI, HeI, and NaI emission lines, clearly reveal the sudden increase of the mass accretion rate. When inspecting the blue arm spectra, the blurry photospheric continuum is hard to be discerned clearly no matter with the single-exposure one, the coadded one, and the coadded smoothed one. We suggest the flux at optical wavelength is dominated by its accretion disk during the outbursts. As pointed out by [Hartmann & Kenyon \(1985\)](#), rapid accretion onto PMS stars may cause the outburst, and emission from the hot, optically thick accretion disk dominates the system light at maximum. We found the direct evidence of outbursts using the LAMOST spectra, supporting the EXor nature proposed by [Antoniucci et al. \(2014\)](#).

Due to the intense emissions originated from the accretion disk, no credible stellar parameter can be determined for #21 using the LAMOST spectra. Because the outbursts and EXor nature were taken into account, we prefer the stellar parameters (T_{eff} as 5718–5209 K, initial mass as 2.1–1.5 M_{\odot} , stellar luminosity as 13–5.4 L_{\odot}) determined by [Antoniucci et al. \(2014\)](#). Moreover, the determined T_{eff} of 5718 K is also consistent with the G-type nature at optical wavelengths during the outbursts suggested by [Hartmann & Kenyon \(1985\)](#). Besides, the G-type assumption is also reasonable according to our blurry photospheric continuum. Thus, we suggest #21 is an outbursting EXor Herbig star, possible precursor of a Herbig Ae star.

#21 is associated with the Perseus Molecular Cloud ([Hsieh & Lai 2013](#); [Evans et al. 2009](#)). According to the parallax provided by Gaia, the determined distance to #21 is about 305.7 pc. As described in Section 5.2, the infrared spectrum reveals the existence of silicate, both amorphous and crystalline. Similarly, [Ábrahám et al.](#)

(2009) detected crystalline forsterite features in the outburst spectrum of EX Lupi, the prototype EXors. They pointed out the crystalline features were not present in quiescence, and concluded that the crystals were produced through thermal annealing in the surface layer of the inner disk by heat from the outburst.

6.2. Comparison with Herbig Ae/Be stars

6.2.1. The NIR and MIR spectral indices

According to the pre-main-sequence evolutionary tracks, most of the F-type PMS stars will eventually become HAeBes. To make a statistic analysis on the disk properties of Herbig stars, we also collected the known HAeBes and their young precursors with determined parameters. Besides our 20 F-type Herbig stars, 429 archival Herbig stars were also retrieved, of which 252 are from [Vioque et al. \(2018\)](#), 128 are from [Vioque et al. \(2022\)](#), and 49 are from [Valegård et al. \(2021\)](#). We obtained infrared photometric data from the AllWISE. We removed sources with ‘dubious’ marks or detected saturations, and finally got 365 Herbig stars with determined parameters for the following statistic analysis.

Not only using the mid-infrared (MIR) spectral index α_{K_S-W3} , we also calculated the near-infrared (NIR) spectral index α_{J-K_S} for each star. NIR emission arises from relatively large dust grains ($\geq 1 \mu\text{m}$ for HAeBes) heated to the sublimation temperature 1500 K at the dust sublimation radius ([Monnier & Millan-Gabet 2002](#)). MIR emission mainly arises from the warm dust. W3 band is most sensitive to 250 K blackbody dust, though contributions from dust with lower or higher temperature can also be present. The uncertainties of the spectral indices were derived from the photometric uncertainties. We plotted the spectral indices versus T_{eff} diagram as shown in Figure 9. The colorbar represents stellar masses. In consideration of the color depth and visual perception, we only presented the 354 stars with stellar masses less than 15 M_{\odot} for better presentation of the lower side. The light red, blue, and green lines ($\alpha_{K_S-W3} = 0.3$, $\alpha_{K_S-W3} = -0.3$, $\alpha_{K_S-W3} = -1.6$, respectively) are the boundaries of the modified 4-class YSO system defined by [Greene et al. \(1994\)](#) (Class I, flat-spectrum class, Class II, and Class III, Section 5.1 for details). The gray lines ($\alpha_{J-K_S} = 0$, $\alpha_{J-K_S} = -2$) in the upper panel are the boundaries of NIR1, NIR2, and NIR3 classes. We divided the Herbig stars into five categories according to T_{eff} . Statistics based on α_{K_S-W3} and α_{J-K_S} are shown as Table 3. Percentages in brackets represent the number ratios of Herbig stars within the same T_{eff} ranges. Considering the uncertainties of T_{eff} , most of the ‘B9 and B9.5’ type Herbig stars may be Herbig Ae stars. Thus, we set the ‘B9 and B9.5’

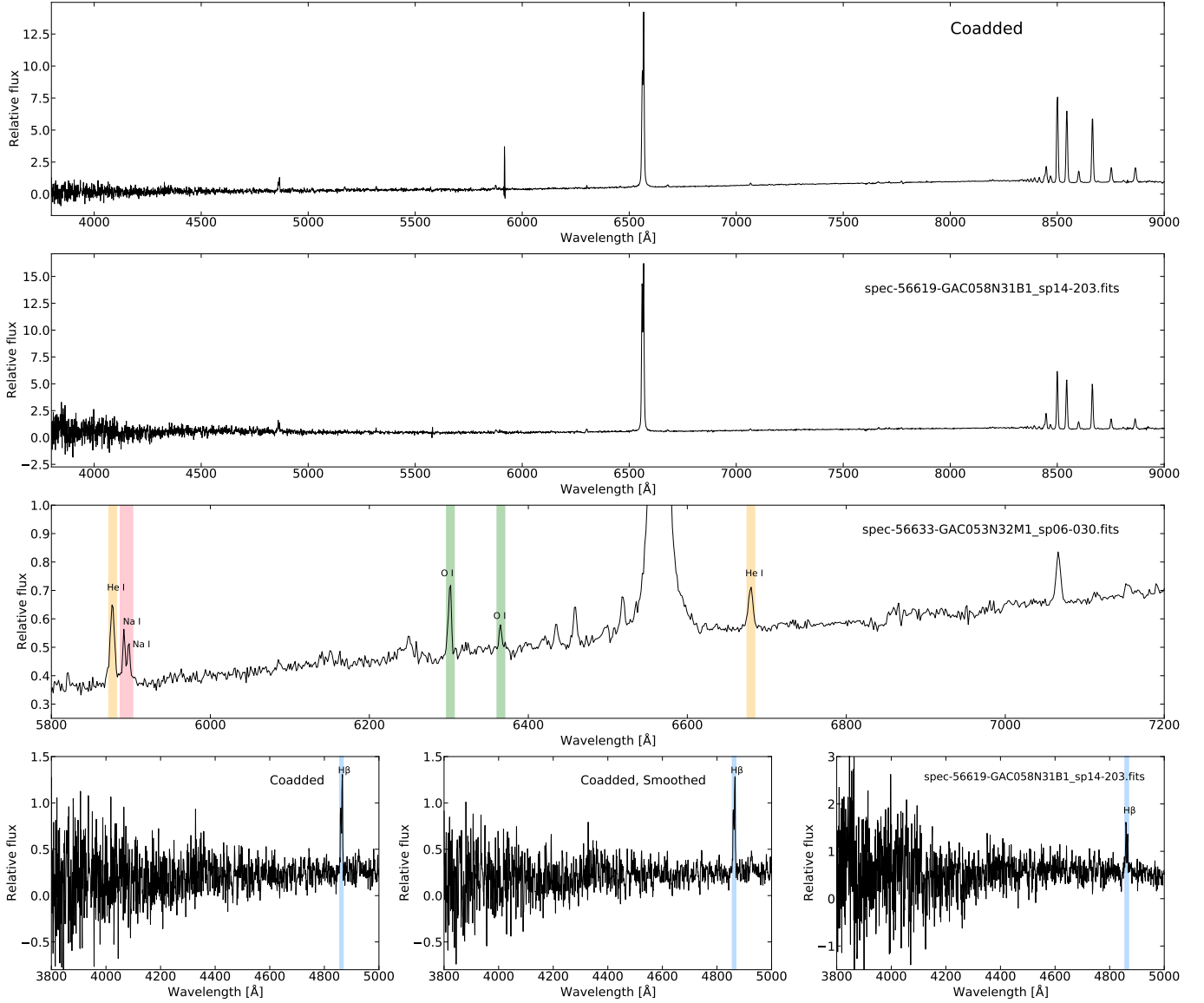


Figure 8. The single-exposure and coadded spectra of #21 J034344.48+314309.3, an outbursting EXor Herbig star, possible precursor of a Herbig Ae star.

type as a separate category in contrast to the ‘B8 and earlier’ type. Intensive discussions on the five categories are presented in the following paragraphs.

As seen in Figure 9 and Table 3, the spectral indices of F-type Herbig stars share the similar distribution with that of G- and K- type Herbig stars. The majority of these precursors (F-, G-, and K- type) have moderate NIR and MIR excesses, and belong to the Class II and NIR2 class. The relative large proportion of the Class III ‘G and K’ type Herbig stars may be due to the small sample size. Besides, except for the proportion of ‘Class I & flat-spectrum class’, the distribution of ‘B9 and B9.5’ type Herbig stars is much more similar to that of Herbig Ae stars than the distribution of ‘B8 and earlier’ type.

There is a trend that the proportion of stars with moderate IR excesses (Class II and NIR2 class) decreases as T_{eff} increases. On the contrary, the proportions of stars with large (Class I & flat-spectrum class and NIR1 class) or little (Class III and NIR3 class) IR excesses increase simultaneously with increasing T_{eff} in general. The trend becomes obvious when compare Herbig Be stars with Herbig Ae stars. Unlike Herbig Ae stars and the precursors, the majority of ‘B8 and earlier’ type Herbig stars have large or little IR excesses instead of the moderate ones. In the 113 ‘B8 and earlier’ type Herbig stars, 28.3% and 42.5% were classified as the Class III and NIR3 class separately (little IR excess), and 39.8% and 30.1% were classified as the ‘Class I & flat-spectrum class’ and NIR1 class separately (large IR excess). More-

over, 25.7% (29/113) were classified as both Class III and NIR1 class, and 22.1% (25/113) were classified as both ‘Class I & flat-spectrum class’ and NIR1 class, in the 113 ‘B8 and earlier’ type Herbig stars. We suspect that the Herbig stars with little IR excesses may likely just reach the main sequence with dust disk dispersed by stellar radiation. The great proportions (28.3% for the Class III and 42.5% for the NIR3 class) are also consistent with the fact that more massive stars evolve much faster and approach the main-sequence phase more quickly.

Hotter Herbig stars tend to have a larger proportion with large IR excesses described as above. It may be due to the fact that hotter stars have larger areas of re-emitting dust, although there is some scatter due to the particularities of each disk. Because of the high stellar luminosity and the intense stellar radiation from Herbig Be stars, distant warm dust may also contribute to the MIR excess. Similarly, the high stellar luminosity of Herbig Be stars also account for the large dust sublimation radius along with the large NIR excess. As revealed by Monnier & Millan-Gabet (2002); Kraus et al. (2008), the NIR emission likely traces dust at the dust sublimation radius in Herbig stars, and the measured NIR sizes are closely related to the stellar luminosity. The high T_{eff} and stellar luminosity usually lead to the large radius of optical thin cavity surrounding the star. Ake et al. (2009) also pointed out that an inflation of the inner disk height naturally leads to a higher NIR excess.

The proportions of precursors with large IR (especially MIR) excesses are much smaller than that of Herbig Ae stars. The only 2 precursors with α_{K_S-W3} above -0.3 were both classified as the flat-spectrum class, without any Class I star. In addition to the cause mentioned above (areas of re-emitting dust), an observational effect may also contribute to it. Those most embedded precursors with large IR excesses and low T_{eff} are hard to be detected in general.

In this work, #13 is the only one with α_{K_S-W3} above -0.3 and its determined T_{eff} is 6900 K. Despite taking a large value of R_V ($R_V = 5$) as suggested by Hernández et al. (2004) for #13 rather than the standard $R_V = 3.1$, we might still underestimate its extinction and luminosity if the real R_V was even larger. Similar to #13, 29 of 32 Herbig stars with T_{eff} around 10,000 K (9500–11,300 K), marked in the red square in Figure 9, have the determined stellar masses less than $3 M_{\odot}$ and were classified as the Class I or the flat-spectrum class. Many of them have the determined ages older than the very young nature indicated by the early stage of disk evolution suggested by Greene et al. (1994); Calvet et al. (1994). It should be noted that disk evolutionary theories are var-

ied and nowadays often present several paths for disk evolution. However, according to the pre-main-sequence evolutionary tracks, the 29 stars are close to the main sequence and should not have, in principle, IR excesses that large. As pointed out by Cardelli et al. (1989), the derived mean extinction law depends on only one parameter, which is chosen to be $R_V \equiv A_V/E(B-V)$. The value of R_V is relevant to the sizes and distributions of dust grains. $R_V = 3.1$ is the standard value for the diffuse interstellar medium and $R_V = 5$ is a value found in some dense clouds. Wang et al. (2004) also pointed out preferential removal of small dust grains such as by coagulation in dense molecular clouds will result in a gray extinction law with large R_V . Hernández et al. (2004) suggested the value of R_V can be used to infer grain properties of the dust surrounding HAeBe stars. We suggest the average Galactic value $R_V = 3.1$ is credible in the less embedded Herbig stars but not the embedded ones. The Herbig stars with extremely large IR excesses (Class I & flat-spectrum class) may be embedded in dense molecular clouds where significant grain growth happens and large size dust grains dominate. We suggest the assumption of $R_V = 3.1$ for the embedded Herbig stars with extremely large IR excesses during the parameter determination in Vioque et al. (2018, 2022) may result in the underestimation of the extinction, stellar luminosity, and mass. Large values of R_V ($R_V = 5$ or larger) should be taken in the cases of ‘Class I & flat-spectrum class’ stars with large IR excesses, and these stars should have larger extinctions and stellar luminosities. According to the pre-main-sequence evolutionary tracks, they should be much younger and more massive than previously thought.

Our simplified indices can trace the general IR trends of Herbig stars rather than the refined disk structures. In fact, the detected disk structures of Herbig stars are complicated, such as cavities, gaps, and spiral arms (Pineda et al. 2019; Uyama et al. 2018; Akiyama et al. 2016). Meeus et al. (2001) defined two groups (Group I and Group II) for HAeBes based on IR excess. The continuum of Group I can be reconstructed by a power-law and a black body, and that of Group II only needs a power-law to fit. MIR excess is dominant and rising for Group I, while moderate and rather descending for Group II. Meeus et al. (2001); Dullemond & Dominik (2004a,b, 2005) suggested Group I may evolve into Group II through grain growth and/or settling. However, Menu et al. (2015); Garufi et al. (2017) argued Group II may involve into Group I through formation of (giant) planets. Recently, Valegård et al. (2021) pointed out Group I and Group II are disconnected and represent two different evolutionary paths.

Moreover, a number of recent work analysed the protoplanetary disks of Herbig stars based on the data from the Atacama Large Millimeter/submillimeter Array (ALMA), the Very Large Telescope Interferometer (VLTI) GRAVITY, and the Gemini- Large Imaging with GPI Herbig/T-tauri Survey (Gemini-LIGHTS) (Rich et al. 2022; Bohn et al. 2022; Stapper et al. 2022; Villenave et al. 2020; Cazzoletti et al. 2019). Results reveal that the dust spatial distributions of Herbig stars are even more complicated and show large star-to-star differences. We simplified the situation and made the statistic analysis of all known Herbig stars with NIR and MIR spectral indices in this section. Considering the complicated situation of Herbig stars, following detailed investigations for individuals are necessary to verify the trends and our speculations mentioned above.

6.2.2. The detection frequency of PAH

Statistic studies reveal a correlation between the detection frequency of PAH and T_{eff} . Acke et al. (2010) found 37 of the 53 Herbig Ae stars (70%) display PAH emission. Keller et al. (2019) pointed out all the 13 HAeBes identified in the Small Magellanic Cloud show PAH emission. Geers et al. (2006) detected PAH features in 3 of the 38 T Tauri stars (8%, with an additional 14 tentative detections). Valegård et al. (2021) pointed out 27% of the 49 IMTT stars show PAH features, and the detection rate becomes 44% when considering tentative detections. In this work, only 4 of the 20 F-type Herbig stars have Spitzer IRS spectra, three of which with T_{eff} about 6400 K display extremely weak PAH emission. As is suggested by Valegård et al. (2021), the detection frequency tends to decrease when the T_{eff} and the UV flux decrease. Despite our small sample, no intense PAH emission detected also supports their suggestion.

7. SUMMARY

In this work, we used the 2.53 million F-type spectra from LAMOST DR8 and identified 20 F-type Herbig stars along with 22 pre-main-sequence candidates. The effective temperature, distance, extinction, stellar luminosity, mass, and radius were derived for each Herbig star based on optical spectra, photometry, Gaia EDR3 parallaxes, and pre-main-sequence evolutionary tracks.

According to SEDs, 19 F-type Herbig stars belong to Class II YSOs, and one belongs to the flat-spectrum class. Four have Spitzer IRS spectra, of which three show extremely weak PAH emissions, and three with both amorphous and crystalline silicate emissions share the similar parameters and are at the same evolutionary stage.

We detected an additional Herbig star J034344.48+314309.3 (R.A. 55.935352, Decl. 31.719259). It was thought to be an EXor, a T Tauri star or a Be star. It is a solar-nearby star with a distance of 305.7 pc. We detected intense emission lines of H I, He I, O I, Na I, and Ca II in its optical spectra, originated from the rapid accretion during the outbursts. We also detected silicate emission features (both amorphous and crystalline) in its infrared spectrum. We suggest it is an outbursting EXor Herbig star, possible precursor of a Herbig Ae star.

We also made a statistic analysis on the disk properties of all known Herbig stars using the defined infrared spectral indices (α_{J-K_S} and α_{K_S-W3}). The possible trends and our speculations are listed as bellow.

1. The spectral indices of F-type Herbig stars share the similar distribution with that of G- and K-type Herbig stars. The majority of these precursors (F-, G-, or K- type) have moderate NIR and MIR excesses, and belong to the Class II and NIR2 class. The distribution of ‘B9 and B9.5’ type Herbig stars is much more similar to that of Herbig Ae stars than the distribution of ‘B8 and earlier’ type.
2. The proportion of Herbig stars with moderate IR excesses decreases as T_{eff} increases. We suspect that the Herbig stars with little IR excesses may likely just reach the main sequence with dust disk dispersed by stellar radiation.
3. Hotter Herbig stars tend to have a larger proportion with large IR excesses. It may be due to the fact that hotter stars have larger areas of re-emitting dust, although there is some scatter due to the particularities of each disk.
4. The proportions of precursors with large IR (especially MIR) excesses are much smaller than that of Herbig Ae stars. In addition to the cause mentioned above (areas of re-emitting dust), an observational effect may also contribute to it. Those most embedded precursors with large IR excesses and low T_{eff} are hard to be detected in general.
5. We suggest the average Galactic value $R_V = 3.1$ is credible in the less embedded Herbig stars but not the embedded ones. Large values of R_V ($R_V = 5$ or larger) should be taken in the cases of ‘Class I & flat-spectrum class’ stars with large IR excesses, and these stars should have larger extinctions and stellar luminosities. According to the pre-main-sequence evolutionary tracks, they

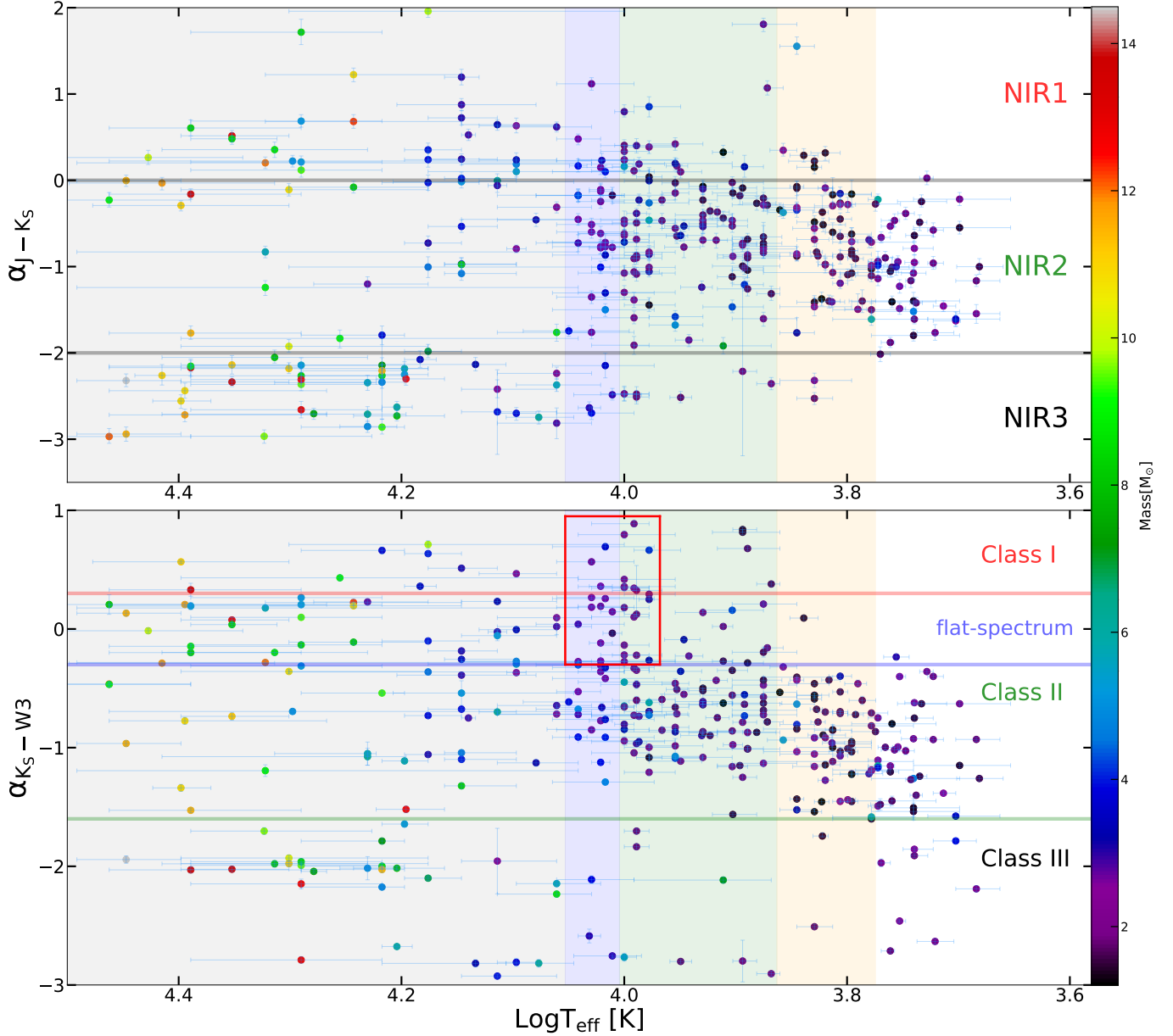


Figure 9. The IR spectral indices of Herbig stars (α_{J-K_S} for the NIR and α_{K_S-W3} for the MIR). The Herbig stars and the determined parameters are from Vioque et al. (2018, 2022); Vælgård et al. (2021) and this work. The colorbar represents stellar masses, and we only presented the 354 stars with stellar masses less than $15 M_{\odot}$ for better presentation of the lower side. The gray lines ($\alpha_{J-K_S} = 0$, $\alpha_{J-K_S} = -2$) in the upper panel are the boundaries of NIR1, NIR2, and NIR3 classes. The light red, blue, and green lines ($\alpha_{K_S-W3} = 0.3$, $\alpha_{K_S-W3} = -0.3$, $\alpha_{K_S-W3} = -1.6$, respectively) in the bottom panel are the boundaries of the modified 4-class YSO system defined by Greene et al. (1994). The background colors of ‘B8 and earlier’, ‘B9 and B9.5’, ‘A’, ‘F’, and ‘G and K’ are set as light gray, blue, green, orange, and white, respectively.

should be much younger and more massive than previously thought.

ACKNOWLEDGEMENTS

We thank the anonymous reviewer and Aigen Li for suggestions and comments that significantly improved the paper. This work is supported by National Science Foundation of China (Nos U1931209, 12003050,

12133002) and National Key R&D Program of China (No. 2019YFA0405502). Guoshoujing Telescope (the Large Sky Area Multi-Object Fiber Spectroscopic Telescope, LAMOST) is a National Major Scientific Project built by the Chinese Academy of Sciences. Funding for the project has been provided by the National Development and Reform Commission. LAMOST is operated and managed by the National Astronomical Ob-

Table 3. Classification of Herbig stars based on α_{K_S-W3} and α_{J-K_S}

Spectral type	T_{eff}	Count	Class I &					
	[K]		flat-spectrum class	Class II	Class III	NIR1	NIR2	NIR3
B8 and earlier	> 11,300	113	45 (39.8%)	36 (31.9%)	32 (28.3%)	34 (30.1%)	31 (27.4%)	48 (42.5%)
B9 and B9.5	10,100–11,300	34	14 (41.2%)	17 (50.0%)	3 (8.8%)	6 (17.6%)	24 (70.6%)	4 (11.8%)
A	7300–10,100	112	32 (28.6%)	73 (65.2%)	7 (6.2%)	22 (19.6%)	83 (74.1%)	7 (6.3%)
F	6000–7300	61	1 (1.6%)	57 (93.5%)	3 (4.9%)	6 (9.8%)	53 (86.9%)	2 (3.3%)
G and K	<6000	45	1 (2.2%)	35 (77.8%)	9 (20.0%)	1 (2.2%)	42 (93.4%)	2 (4.4%)

NOTE—The ‘Count’ column is the total number of Herbig stars with corresponding spectral types and T_{eff} . Columns 4–9 show the counts of Herbig stars with specified classes. Percentages in brackets are the number ratios of Herbig stars within the same T_{eff} ranges. The 4-class system (Class I, flat-spectrum class, Class II, Class III) is based on α_{K_S-W3} , and the 3-class one (NIR1, NIR2, NIR3) is based on α_{J-K_S} .

servatories, Chinese Academy of Sciences. This publication makes use of data products from the Wide-field Infrared Survey Explorer, which is a joint project of the University of California, Los Angeles, and the Jet Propulsion Laboratory/California Institute of Technology, funded by the National Aeronautics and Space Administration. This research makes use of data from the European Space Agency (ESA) mission Gaia, processed by the Gaia Data Processing and Analysis Consortium. This publication makes use of VOSA, developed under the Spanish Virtual Observatory project funded

by MCIN/AEI/10.13039/501100011033/ through grant PID2020-112949GB-I00. VOSA has been partially updated by using funding from the European Union’s Horizon 2020 Research and Innovation Programme, under Grant Agreement n° 776403 (EXOPLANETS-A). This research also makes use of Astropy, a community-developed core Python package for Astronomy (Astropy Collaboration et al. 2013), the TOPCAT tool (Taylor 2005) and the VizieR catalog access tool and the Simbad database, operated at CDS, Strasbourg, France.

APPENDIX

A. PRE-MAIN-SEQUENCE CANDIDATES

Data for the 22 Pre-main-sequence candidates is provided in Table A.

REFERENCES

- 1988a, Infrared Astronomical Satellite (IRAS) Catalogs and Atlases. Volume 1: Explanatory Supplement., Vol. 1
- 1988b, Infrared Astronomical Satellite (IRAS) Catalogs and Atlases. Volume 7: The Small Scale Structure Catalog., Vol. 7
- Ábrahám, P., Juhász, A., Dullemond, C. P., et al. 2009, *Nature*, 459, 224, doi: [10.1038/nature08004](https://doi.org/10.1038/nature08004)
- Acke, B., Bouwman, J., Juhász, A., et al. 2010, *ApJ*, 718, 558, doi: [10.1088/0004-637X/718/1/558](https://doi.org/10.1088/0004-637X/718/1/558)
- Acke, B., Min, M., van den Ancker, M. E., et al. 2009, *A&A*, 502, L17, doi: [10.1051/0004-6361/200912728](https://doi.org/10.1051/0004-6361/200912728)
- Acke, B., & van den Ancker, M. E. 2006, *A&A*, 457, 171, doi: [10.1051/0004-6361:20065612](https://doi.org/10.1051/0004-6361:20065612)
- Akiyama, E., Hashimoto, J., Liu, H. B., et al. 2016, *AJ*, 152, 222, doi: [10.3847/1538-3881/152/6/222](https://doi.org/10.3847/1538-3881/152/6/222)
- Alecian, E., Wade, G. A., Catala, C., et al. 2013, *MNRAS*, 429, 1001, doi: [10.1093/mnras/sts383](https://doi.org/10.1093/mnras/sts383)
- Andre, P., Ward-Thompson, D., & Barsony, M. 1993, *ApJ*, 406, 122, doi: [10.1086/172425](https://doi.org/10.1086/172425)
- Antoniucci, S., Giannini, T., Li Causi, G., & Lorenzetti, D. 2014, *ApJ*, 782, 51, doi: [10.1088/0004-637X/782/1/51](https://doi.org/10.1088/0004-637X/782/1/51)
- Astropy Collaboration, Robitaille, T. P., Tollerud, E. J., et al. 2013, *A&A*, 558, A33, doi: [10.1051/0004-6361/201322068](https://doi.org/10.1051/0004-6361/201322068)
- Azimlu, M., Martínez-Galarza, J. R., & Muench, A. A. 2015, *AJ*, 150, 95, doi: [10.1088/0004-6256/150/3/95](https://doi.org/10.1088/0004-6256/150/3/95)
- Bai, Z.-R., Zhang, H.-T., Yuan, H.-L., et al. 2017, *Research in Astronomy and Astrophysics*, 17, 091, doi: [10.1088/1674-4527/17/9/91](https://doi.org/10.1088/1674-4527/17/9/91)

Table A. Pre-main-sequence candidates

No.	Designation	R.A. [degree]	Decl. [degree]	Specname
C1	J032025.39+554621.1	50.105798	55.772531	spec-56937-HD032616N560830V01_sp03-031.fits
C2	J034512.81+521437.7	56.303389	52.243824	spec-55903-B90304_sp11-014.fits
C3	J034714.72+472557.6	56.811339	47.432686	spec-56627-GAC056N46V1_sp09-088.fits
C4	J044319.47+445421.7	70.831162	44.906046	spec-57425-GAC067N44B3_sp13-045.fits
C5	J051905.92+383946.8	79.774677	38.663002	spec-57015-GAC082N38M1_sp14-233.fits
C6	J053304.15+384300.9	83.267325	38.716921	spec-55976-GAC_084N40_V1_sp05-223.fits
C7	J053715.40+244917.2	84.314167	24.821472	spec-56271-GAC084N26B1_sp01-054.fits
C8	J053813.35+274047.1	84.555634	27.67975	spec-55918-GAC_082N29_M1_sp07-094.fits
C9	J054022.60+355913.0	85.094182	35.986965	spec-57328-GAC084N35B1_sp09-202.fits
C10	J054950.53+270701.4	87.460583	27.117083	spec-55876-GAC_089N28_B1_sp02-147.fits
C11	J055018.51+281042.6	87.577164	28.178522	spec-55876-GAC_089N28_B1_sp10-167.fits
C12	J055532.35+274451.3	88.884792	27.747611	spec-55892-GAC_082N27_M1_sp09-147.fits
C13	J055801.69+192238.7	89.507083	19.377417	spec-56648-GAC088N20B1_sp08-116.fits
C14	J055828.98+264039.9	89.620756	26.677767	spec-55892-GAC_082N27_M1_sp06-207.fits
C15	J060413.19+211639.6	91.054997	21.277676	spec-56595-GAC088N22M1_sp07-143.fits
C16	J061136.87+203104.0	92.903638	20.517795	spec-57753-GAC093N19M2_sp15-198.fits
C17	J061141.85+203158.9	92.924376	20.533032	spec-57753-GAC093N19M2_sp15-193.fits
C18	J061624.46+241837.1	94.101938	24.310332	spec-57009-GAC091N23M1_sp13-002.fits
C19	J063144.07+021335.0	97.933625	2.2263889	spec-58137-GAC099N02B2_sp10-211.fits
C20	J063146.08+044228.8	97.942032	4.7080234	spec-55976-GAC_099N04_V5_sp10-243.fits
C21	J063856.02+542940.4	99.733451	54.49457	spec-57814-GAC101N53M1_sp16-164.fits
C22	J212547.34-022251.2	321.447259	-2.380904	spec-57641-EG213415S032438V01_sp14-106.fits

NOTE—The ‘No.’ column is the sequential identifier of the 22 Pre-main-sequence candidates. The ‘Specname’ column is the FITS name of each spectrum.

- Bailer-Jones, C. A. L., Rybizki, J., Fouesneau, M., Demleitner, M., & Andrae, R. 2021, *AJ*, 161, 147, doi: [10.3847/1538-3881/abd806](https://doi.org/10.3847/1538-3881/abd806)
- Baines, D., Oudmaijer, R. D., Porter, J. M., & Pozzo, M. 2006, *MNRAS*, 367, 737, doi: [10.1111/j.1365-2966.2006.10006.x](https://doi.org/10.1111/j.1365-2966.2006.10006.x)
- Banzatti, A., & Pontoppidan, K. M. 2015, *ApJ*, 809, 167, doi: [10.1088/0004-637X/809/2/167](https://doi.org/10.1088/0004-637X/809/2/167)
- Bastian, U., Finkenzeller, U., Jaschek, C., & Jaschek, M. 1983, *A&A*, 126, 438
- Beichman, C. A., Boulanger, F., & Moshir, M. 1992, *ApJ*, 386, 248, doi: [10.1086/171011](https://doi.org/10.1086/171011)
- Bohn, A. J., Benisty, M., Perraut, K., et al. 2022, *A&A*, 658, A183, doi: [10.1051/0004-6361/202142070](https://doi.org/10.1051/0004-6361/202142070)
- Bollen, D., Kamath, D., Van Winckel, H., & De Marco, O. 2019, *A&A*, 631, A53, doi: [10.1051/0004-6361/201936073](https://doi.org/10.1051/0004-6361/201936073)
- Bressan, A., Marigo, P., Girardi, L., et al. 2012, *MNRAS*, 427, 127, doi: [10.1111/j.1365-2966.2012.21948.x](https://doi.org/10.1111/j.1365-2966.2012.21948.x)
- Calvet, N., Hartmann, L., Kenyon, S. J., & Whitney, B. A. 1994, *ApJ*, 434, 330, doi: [10.1086/174731](https://doi.org/10.1086/174731)
- Calvet, N., Muzerolle, J., Briceño, C., et al. 2004, *AJ*, 128, 1294, doi: [10.1086/422733](https://doi.org/10.1086/422733)
- Cardelli, J. A., Clayton, G. C., & Mathis, J. S. 1989, *ApJ*, 345, 245, doi: [10.1086/167900](https://doi.org/10.1086/167900)
- Carmona, A., van den Ancker, M. E., Audard, M., et al. 2010, *A&A*, 517, A67, doi: [10.1051/0004-6361/200913800](https://doi.org/10.1051/0004-6361/200913800)
- Casali, M. M., & Eiroa, C. 1996, *A&A*, 306, 427
- Castelli, F., & Kurucz, R. L. 2003, in *Modelling of Stellar Atmospheres*, ed. N. Piskunov, W. W. Weiss, & D. F. Gray, Vol. 210, A20. <https://arxiv.org/abs/astro-ph/0405087>
- Cazzoletti, P., Manara, C. F., Liu, H. B., et al. 2019, *A&A*, 626, A11, doi: [10.1051/0004-6361/201935273](https://doi.org/10.1051/0004-6361/201935273)
- Chen, P. S., Shan, H. G., & Zhang, P. 2016, *NewA*, 44, 1, doi: [10.1016/j.newast.2015.09.001](https://doi.org/10.1016/j.newast.2015.09.001)
- Chojnowski, S. D., Whelan, D. G., Wisniewski, J. P., et al. 2015, *AJ*, 149, 7, doi: [10.1088/0004-6256/149/1/7](https://doi.org/10.1088/0004-6256/149/1/7)
- Chojnowski, S. D., Wisniewski, J. P., Whelan, D. G., et al. 2017, *AJ*, 153, 174, doi: [10.3847/1538-3881/aa64ce](https://doi.org/10.3847/1538-3881/aa64ce)
- Cottaar, M., Covey, K. R., Meyer, M. R., et al. 2014, *ApJ*, 794, 125, doi: [10.1088/0004-637X/794/2/125](https://doi.org/10.1088/0004-637X/794/2/125)

- Cutri, R. M., Skrutskie, M. F., van Dyk, S., et al. 2003, *VizieR Online Data Catalog*, II/246
- Dullemond, C. P., & Dominik, C. 2004a, *A&A*, 417, 159, doi: [10.1051/0004-6361:20031768](https://doi.org/10.1051/0004-6361:20031768)
- . 2004b, *A&A*, 421, 1075, doi: [10.1051/0004-6361:20040284](https://doi.org/10.1051/0004-6361:20040284)
- . 2005, *A&A*, 434, 971, doi: [10.1051/0004-6361:20042080](https://doi.org/10.1051/0004-6361:20042080)
- Evans, Neal J., I., Dunham, M. M., Jørgensen, J. K., et al. 2009, *ApJS*, 181, 321, doi: [10.1088/0067-0049/181/2/321](https://doi.org/10.1088/0067-0049/181/2/321)
- Fairlamb, J. R., Oudmaijer, R. D., Mendigutía, I., Ilee, J. D., & van den Ancker, M. E. 2015, *MNRAS*, 453, 976, doi: [10.1093/mnras/stv1576](https://doi.org/10.1093/mnras/stv1576)
- Finkenzeller, U., & Mundt, R. 1984, *A&AS*, 55, 109
- Garufi, A., Meeus, G., Benisty, M., et al. 2017, *A&A*, 603, A21, doi: [10.1051/0004-6361/201630320](https://doi.org/10.1051/0004-6361/201630320)
- Geers, V. C., Augereau, J. C., Pontoppidan, K. M., et al. 2006, *A&A*, 459, 545, doi: [10.1051/0004-6361:20064830](https://doi.org/10.1051/0004-6361:20064830)
- Gray, R. O., & Corbally, Christopher, J. 2009, *Stellar Spectral Classification*
- Greene, T. P., Wilking, B. A., Andre, P., Young, E. T., & Lada, C. J. 1994, *ApJ*, 434, 614, doi: [10.1086/174763](https://doi.org/10.1086/174763)
- Gregorio-Hetem, J., Lepine, J. R. D., Quast, G. R., Torres, C. A. O., & de La Reza, R. 1992, *AJ*, 103, 549, doi: [10.1086/116082](https://doi.org/10.1086/116082)
- Gutermuth, R. A., Megeath, S. T., Myers, P. C., et al. 2009, *ApJS*, 184, 18, doi: [10.1088/0067-0049/184/1/18](https://doi.org/10.1088/0067-0049/184/1/18)
- Guzmán-Díaz, J., Mendigutía, I., Montesinos, B., et al. 2021, *A&A*, 650, A182, doi: [10.1051/0004-6361/202039519](https://doi.org/10.1051/0004-6361/202039519)
- Hartmann, L., & Kenyon, S. J. 1985, *ApJ*, 299, 462, doi: [10.1086/163713](https://doi.org/10.1086/163713)
- Hein Bertelsen, R. P., Kamp, I., van der Plas, G., et al. 2016, *A&A*, 590, A98, doi: [10.1051/0004-6361/201527652](https://doi.org/10.1051/0004-6361/201527652)
- Heinze, A. N., Tonry, J. L., Denneau, L., et al. 2018, *AJ*, 156, 241, doi: [10.3847/1538-3881/aae47f](https://doi.org/10.3847/1538-3881/aae47f)
- Henden, A. A., Templeton, M., Terrell, D., et al. 2016, *VizieR Online Data Catalog*, II/336
- Herbig, G. H. 1960, *ApJS*, 4, 337, doi: [10.1086/190050](https://doi.org/10.1086/190050)
- . 1962, *Advances in Astronomy and Astrophysics*, 1, 47, doi: [10.1016/B978-1-4831-9919-1.50006-6](https://doi.org/10.1016/B978-1-4831-9919-1.50006-6)
- . 1977, *ApJ*, 214, 747, doi: [10.1086/155304](https://doi.org/10.1086/155304)
- Hernández, J., Calvet, N., Briceño, C., Hartmann, L., & Berlind, P. 2004, *AJ*, 127, 1682, doi: [10.1086/381908](https://doi.org/10.1086/381908)
- Hernández, J., Calvet, N., Hartmann, L., et al. 2005, *AJ*, 129, 856, doi: [10.1086/426918](https://doi.org/10.1086/426918)
- Houck, J. R., Roellig, T. L., van Cleve, J., et al. 2004, *ApJS*, 154, 18, doi: [10.1086/423134](https://doi.org/10.1086/423134)
- Hsieh, T.-H., & Lai, S.-P. 2013, *ApJS*, 205, 5, doi: [10.1088/0067-0049/205/1/5](https://doi.org/10.1088/0067-0049/205/1/5)
- Ishihara, D., Onaka, T., Kataza, H., et al. 2010, *A&A*, 514, A1, doi: [10.1051/0004-6361/200913811](https://doi.org/10.1051/0004-6361/200913811)
- Joy, A. H. 1945, *ApJ*, 102, 168, doi: [10.1086/144749](https://doi.org/10.1086/144749)
- Keller, L. D., Sloan, G. C., Oliveira, J. M., et al. 2019, *ApJ*, 878, 147, doi: [10.3847/1538-4357/ab204a](https://doi.org/10.3847/1538-4357/ab204a)
- Kenyon, S. J., Hartmann, L. W., Strom, K. M., & Strom, S. E. 1990, *AJ*, 99, 869, doi: [10.1086/115380](https://doi.org/10.1086/115380)
- Koenig, X. P., & Leisawitz, D. T. 2014, *ApJ*, 791, 131, doi: [10.1088/0004-637X/791/2/131](https://doi.org/10.1088/0004-637X/791/2/131)
- Kraemer, K. E., Shipman, R. F., Price, S. D., et al. 2003, *AJ*, 126, 1423, doi: [10.1086/377522](https://doi.org/10.1086/377522)
- Kraus, S., Hofmann, K. H., Benisty, M., et al. 2008, *A&A*, 489, 1157, doi: [10.1051/0004-6361:200809946](https://doi.org/10.1051/0004-6361:200809946)
- Lada, C. J. 1987, in *Star Forming Regions*, ed. M. Peimbert & J. Jugaku, Vol. 115, 1
- Lavail, A., Kochukhov, O., Hussain, G. A. J., et al. 2017, *A&A*, 608, A77, doi: [10.1051/0004-6361/201731889](https://doi.org/10.1051/0004-6361/201731889)
- Lee, H.-T., & Chen, W. P. 2007, *ApJ*, 657, 884, doi: [10.1086/510893](https://doi.org/10.1086/510893)
- Lindegren, L., Klioner, S. A., Hernández, J., et al. 2021, *A&A*, 649, A2, doi: [10.1051/0004-6361/202039709](https://doi.org/10.1051/0004-6361/202039709)
- Luo, A. L., Zhao, Y.-H., Zhao, G., et al. 2015, *Research in Astronomy and Astrophysics*, 15, 1095, doi: [10.1088/1674-4527/15/8/002](https://doi.org/10.1088/1674-4527/15/8/002)
- Manoj, P., Bhatt, H. C., Maheswar, G., & Muneer, S. 2006, *ApJ*, 653, 657, doi: [10.1086/508764](https://doi.org/10.1086/508764)
- Marigo, P., Girardi, L., Bressan, A., et al. 2017, *ApJ*, 835, 77, doi: [10.3847/1538-4357/835/1/77](https://doi.org/10.3847/1538-4357/835/1/77)
- Marton, G., Abraham, P., Szegedi-Elek, E., et al. 2019, *MNRAS*, 487, 2522, doi: [10.1093/mnras/stz1301](https://doi.org/10.1093/mnras/stz1301)
- Meeus, G., Waters, L. B. F. M., Bouwman, J., et al. 2001, *A&A*, 365, 476, doi: [10.1051/0004-6361:20000144](https://doi.org/10.1051/0004-6361:20000144)
- Menu, J., van Boekel, R., Henning, T., et al. 2015, *A&A*, 581, A107, doi: [10.1051/0004-6361/201525654](https://doi.org/10.1051/0004-6361/201525654)
- Monnier, J. D., & Millan-Gabet, R. 2002, *ApJ*, 579, 694, doi: [10.1086/342917](https://doi.org/10.1086/342917)
- Montesinos, B., Eiroa, C., Mora, A., & Merín, B. 2009, *A&A*, 495, 901, doi: [10.1051/0004-6361:200810623](https://doi.org/10.1051/0004-6361:200810623)
- Moura, T., Alencar, S. H. P., Sousa, A. P., Alecian, E., & Lebreton, Y. 2020, *MNRAS*, 494, 3512, doi: [10.1093/mnras/staa695](https://doi.org/10.1093/mnras/staa695)
- Núñez, E. H., Povich, M. S., Binder, B. A., Townsley, L. K., & Broos, P. S. 2021, *AJ*, 162, 153, doi: [10.3847/1538-3881/ac0af8](https://doi.org/10.3847/1538-3881/ac0af8)
- Olofsson, J., Augereau, J. C., van Dishoeck, E. F., et al. 2009, *A&A*, 507, 327, doi: [10.1051/0004-6361/200912062](https://doi.org/10.1051/0004-6361/200912062)
- Oomen, G.-M., Van Winckel, H., Pols, O., & Nelemans, G. 2019, *A&A*, 629, A49, doi: [10.1051/0004-6361/201935853](https://doi.org/10.1051/0004-6361/201935853)
- Pecaut, M. J., & Mamajek, E. E. 2013, *ApJS*, 208, 9, doi: [10.1088/0067-0049/208/1/9](https://doi.org/10.1088/0067-0049/208/1/9)

- Pereira, C. B., Miranda, L. F., & Marcolino, W. L. F. 2021, *AJ*, 162, 71, doi: [10.3847/1538-3881/abfe65](https://doi.org/10.3847/1538-3881/abfe65)
- Pineda, J. E., Szulágyi, J., Quanz, S. P., et al. 2019, *ApJ*, 871, 48, doi: [10.3847/1538-4357/aaf389](https://doi.org/10.3847/1538-4357/aaf389)
- Rebull, L. M., Koenig, X. P., Padgett, D. L., et al. 2011, *ApJS*, 196, 4, doi: [10.1088/0067-0049/196/1/4](https://doi.org/10.1088/0067-0049/196/1/4)
- Rich, E. A., Monnier, J. D., Aarnio, A., et al. 2022, arXiv e-prints, arXiv:2206.05815.
<https://arxiv.org/abs/2206.05815>
- Riello, M., De Angeli, F., Evans, D. W., et al. 2021, *A&A*, 649, A3, doi: [10.1051/0004-6361/202039587](https://doi.org/10.1051/0004-6361/202039587)
- Sartori, M. J., Gregorio-Hetem, J., Rodrigues, C. V., Hetem, Annibal, J., & Batalha, C. 2010, *AJ*, 139, 27, doi: [10.1088/0004-6256/139/1/27](https://doi.org/10.1088/0004-6256/139/1/27)
- Seok, J. Y., & Li, A. 2017, *ApJ*, 835, 291, doi: [10.3847/1538-4357/835/2/291](https://doi.org/10.3847/1538-4357/835/2/291)
- Skrutskie, M. F., Cutri, R. M., Stiening, R., et al. 2006, *AJ*, 131, 1163, doi: [10.1086/498708](https://doi.org/10.1086/498708)
- Stapper, L. M., Hogerheijde, M. R., van Dishoeck, E. F., & Mentel, R. 2022, *A&A*, 658, A112, doi: [10.1051/0004-6361/202142164](https://doi.org/10.1051/0004-6361/202142164)
- Strom, S. E., Strom, K. M., Yost, J., Carrasco, L., & Grasdalen, G. 1972, *ApJ*, 173, 353, doi: [10.1086/151425](https://doi.org/10.1086/151425)
- Taylor, M. B. 2005, in *Astronomical Society of the Pacific Conference Series*, Vol. 347, *Astronomical Data Analysis Software and Systems XIV*, ed. P. Shopbell, M. Britton, & R. Ebert, 29
- The, P. S., de Winter, D., & Perez, M. R. 1994, *A&AS*, 104, 315
- Tognelli, E., Prada Moroni, P. G., & Degl'Innocenti, S. 2011, *A&A*, 533, A109, doi: [10.1051/0004-6361/200913913](https://doi.org/10.1051/0004-6361/200913913)
- Torres, C. A. O., Quast, G., de La Reza, R., Gregorio-Hetem, J., & Lepine, J. R. D. 1995, *AJ*, 109, 2146, doi: [10.1086/117440](https://doi.org/10.1086/117440)
- Uyama, T., Hashimoto, J., Muto, T., et al. 2018, *AJ*, 156, 63, doi: [10.3847/1538-3881/aacbd1](https://doi.org/10.3847/1538-3881/aacbd1)
- Valegård, P. G., Waters, L. B. F. M., & Dominik, C. 2021, *A&A*, 652, A133, doi: [10.1051/0004-6361/202039802](https://doi.org/10.1051/0004-6361/202039802)
- Varga, J., Ábrahám, P., Chen, L., et al. 2018, *A&A*, 617, A83, doi: [10.1051/0004-6361/201832599](https://doi.org/10.1051/0004-6361/201832599)
- Vieira, S. L. A., Corradi, W. J. B., Alencar, S. H. P., et al. 2003, *AJ*, 126, 2971, doi: [10.1086/379553](https://doi.org/10.1086/379553)
- Villebrun, F., Alecian, E., Hussain, G., et al. 2019, *A&A*, 622, A72, doi: [10.1051/0004-6361/201833545](https://doi.org/10.1051/0004-6361/201833545)
- Villeneuve, M., Ménard, F., Dent, W. R. F., et al. 2020, *A&A*, 642, A164, doi: [10.1051/0004-6361/202038087](https://doi.org/10.1051/0004-6361/202038087)
- Vioque, M., Oudmaijer, R. D., Baines, D., Mendigutía, I., & Pérez-Martínez, R. 2018, *A&A*, 620, A128, doi: [10.1051/0004-6361/201832870](https://doi.org/10.1051/0004-6361/201832870)
- Vioque, M., Oudmaijer, R. D., Schreiner, M., et al. 2020, *A&A*, 638, A21, doi: [10.1051/0004-6361/202037731](https://doi.org/10.1051/0004-6361/202037731)
- Vioque, M., Oudmaijer, R. D., Wichittanakom, C., et al. 2022, *ApJ*, 930, 39, doi: [10.3847/1538-4357/ac5c46](https://doi.org/10.3847/1538-4357/ac5c46)
- Wang, J., Hall, P. B., Ge, J., Li, A., & Schneider, D. P. 2004, *ApJ*, 609, 589, doi: [10.1086/421240](https://doi.org/10.1086/421240)
- Wang, S., & Chen, X. 2019, *ApJ*, 877, 116, doi: [10.3847/1538-4357/ab1c61](https://doi.org/10.3847/1538-4357/ab1c61)
- Wei, P., Luo, A., Li, Y., et al. 2014, *AJ*, 147, 101, doi: [10.1088/0004-6256/147/5/101](https://doi.org/10.1088/0004-6256/147/5/101)
- Weintraub, D. A. 1990, *ApJS*, 74, 575, doi: [10.1086/191509](https://doi.org/10.1086/191509)
- Werner, M. W., Roellig, T. L., Low, F. J., et al. 2004, *ApJS*, 154, 1, doi: [10.1086/422992](https://doi.org/10.1086/422992)
- Wichittanakom, C., Oudmaijer, R. D., Fairlamb, J. R., et al. 2020, *MNRAS*, 493, 234, doi: [10.1093/mnras/staa169](https://doi.org/10.1093/mnras/staa169)
- Wright, E. L., Eisenhardt, P. R. M., Mainzer, A. K., et al. 2010, *AJ*, 140, 1868, doi: [10.1088/0004-6256/140/6/1868](https://doi.org/10.1088/0004-6256/140/6/1868)
- . 2013, doi: [10.26131/IRSA1](https://doi.org/10.26131/IRSA1)
- Xue, M., Jiang, B. W., Gao, J., et al. 2016, *ApJS*, 224, 23, doi: [10.3847/0067-0049/224/2/23](https://doi.org/10.3847/0067-0049/224/2/23)
- Zacharias, N., Finch, C. T., Girard, T. M., et al. 2012, *VizieR Online Data Catalog*, I/322A
- Zhang, P., Yang, H. T., & Liu, J. 2006, *Ap&SS*, 305, 11, doi: [10.1007/s10509-005-9031-6](https://doi.org/10.1007/s10509-005-9031-6)
- Zhang, Y.-J., Hou, W., Luo, A. L., et al. 2022, *ApJS*, 259, 38, doi: [10.3847/1538-4365/ac4964](https://doi.org/10.3847/1538-4365/ac4964)